

**Repository of the Max Delbrück Center for Molecular Medicine (MDC)
in the Helmholtz Association**

<http://edoc.mdc-berlin.de/10993>

Mutant huntingtin impairs Ku70-mediated DNA repair


Enokido, Y. and Tamura, T. and Ito, H. and Arumughan, A. and Komuro, A. and Shiwaku, H. and Sone, M. and Foulle, R. and Sawada, H. and Ishiguro, H. and Ono, T. and Murata, M. and Kanazawa, I. and Tomilin, N. and Tagawa, K. and Wanker, E.E. and Okazawa, H.

This is a copy of the final article, which was first published online on 03 May 2010 and in final edited form in:

Journal of Cell Biology
2010 MAY 03 ; 189(3): 425-443
doi: [10.1083/jcb.200905138](https://doi.org/10.1083/jcb.200905138)

Publisher: [Rockefeller University Press](http://www.rupress.org)

© 2010 Enokido et al. This article is distributed under the terms of an Attribution–Noncommercial–Share Alike–No Mirror Sites license for the first six months after the publication date (see <http://www.rupress.org/terms>).

 After six months it is available under a Creative Commons License (Attribution–Noncommercial–Share Alike 3.0 Unported license, as described at <http://creativecommons.org/licenses/by-nc-sa/3.0/>).

Mutant huntingtin impairs Ku70-mediated DNA repair

Yasushi Enokido,¹ Takuya Tamura,¹ Hikaru Ito,¹ Anup Arumughan,² Akihiko Komuro,¹ Hiroki Shiwaku,¹ Masaki Sone,¹ Raphael Foulle,² Hirohide Sawada,³ Hiroshi Ishiguro,⁴ Tetsuya Ono,⁵ Miho Murata,⁶ Ichiro Kanazawa,⁶ Nikolai Tomilin,⁷ Kazuhiko Tagawa,¹ Erich E. Wanker,² and Hitoshi Okazawa^{1,8}

¹Department of Neuropathology, Medical Research Institute, Tokyo Medical and Dental University, Bunkyo-ku, Tokyo 113-8510, Japan

²Department of Neurogenetics, Max-Delbrück Center for Molecular Medicine, 13125 Berlin-Buch, Germany

³Department of Clinical Technology, Kobe Takiwa University, Osada-ku, Kobe 653-0838, Japan

⁴Carna Biosciences, Chuo-ku, Kobe, 650-0047, Japan

⁵Department of Genome Biology, Tohoku University, Seiryō-cho, Sendai 980-8575, Japan

⁶National Center for Neurology and Psychiatry, Kodaira, Tokyo 187-8502, Japan

⁷Institute of Cytology RAS, St. Petersburg 194064, Russia

⁸Japan Science and Technology Agency, PRESTO, Core Research for Evolutional Science and Technology (CREST), Kawaguchi 332-0012, Japan

DNA repair defends against naturally occurring or disease-associated DNA damage during the long lifespan of neurons and is implicated in polyglutamine disease pathology. In this study, we report that mutant huntingtin (Htt) expression in neurons causes double-strand breaks (DSBs) of genomic DNA, and Htt further promotes DSBs by impairing DNA repair. We identify Ku70, a component of the DNA damage repair complex, as a mediator of the

DNA repair dysfunction in mutant Htt-expressing neurons. Mutant Htt interacts with Ku70, impairs DNA-dependent protein kinase function in nonhomologous end joining, and consequently increases DSB accumulation. Expression of exogenous Ku70 rescues abnormal behavior and pathological phenotypes in the R6/2 mouse model of Huntington's disease (HD). These results collectively suggest that Ku70 is a critical regulator of DNA damage in HD pathology.

Introduction

Multiple cellular dysfunctions underlie the molecular pathology of polyglutamine (polyQ) diseases, including Huntington's disease (HD) and various spinocerebellar ataxias, which compose a major group of hereditary neurodegenerative disorders. Various cellular functions, including transcription (Okazawa et al., 2002; Sugars and Rubinsztein, 2003; Butler and Bates, 2006; Ross and Thompson, 2006), splicing (Jackson et al., 1998; Shibata et al., 2000; Waragai et al., 2000), proteasome activity (Johnston et al., 1998; Venkatraman et al., 2004; Bennett et al., 2007), autophagy (Ravikumar et al., 2004; Iwata et al., 2005; Pandey et al., 2007), axonal transport (Gauthier et al., 2004), synaptic transmission (Li et al., 2000, 2004; Murphy et al., 2000),

endocytosis (Metzler et al., 2001; Singaraja et al., 2002), mitochondrial membrane stability (Panov et al., 2002; Ruan et al., 2004), energy metabolism (Cui et al., 2006; St-Pierre et al., 2006; Weydt et al., 2006), and oxidative stress response (Wytenbach et al., 2002; Giorgini et al., 2005; for review see Lin and Beal, 2006), are affected in neurons expressing mutant polyQ proteins. Understanding of these pathogenic pathways is definitely necessary for developing therapeutics (Di Prospero and Fischbeck, 2005; Soong and Paulson, 2007).

In addition to these, activation of genotoxic stress signaling has recently emerged as a new fundamental pathology (Giuliano et al., 2003; Qi et al., 2007). This hypothesis was derived from the observation that two critical mediators of the genotoxic stress signal pathway, p53 and p73, are activated in cultured cells and mouse models expressing mutant huntingtin (Htt) protein (Steffan et al., 2000; Bae et al., 2005;

Y. Enokido, T. Tamura, and H. Ito contributed equally to this paper.

Correspondence to Hitoshi Okazawa: okazawa-ky@umin.ac.jp

Abbreviations used in this paper: ATM, ataxia telangiectasia mutated; CPT, camptothecin; DSB, double-strand break; DNA-PK, DNA-dependent protein kinase; DNA-PKcs, DNA-PK catalytic subunit; ERK, extracellular-regulated kinase; HD, Huntington's disease; Htt, huntingtin; IP, immunoprecipitation; NHEJ, nonhomologous end joining; NSE, neuron-specific enolase; polyQ, polyglutamine; shRNA, short hairpin RNA; SSB, single-strand break; Top1, topoisomerase I.

© 2010 Enokido et al. This article is distributed under the terms of an Attribution-Noncommercial-Share Alike-No Mirror Sites license for the first six months after the publication date [see <http://www.rupress.org/terms>]. After six months it is available under a Creative Commons License [Attribution-Noncommercial-Share Alike 3.0 Unported license, as described at <http://creativecommons.org/licenses/by-nc-sa/3.0/>].

Supplemental Material can be found at:
<http://jcb.rupress.org/content/suppl/2010/04/30/jcb.200905138.DC1.html>

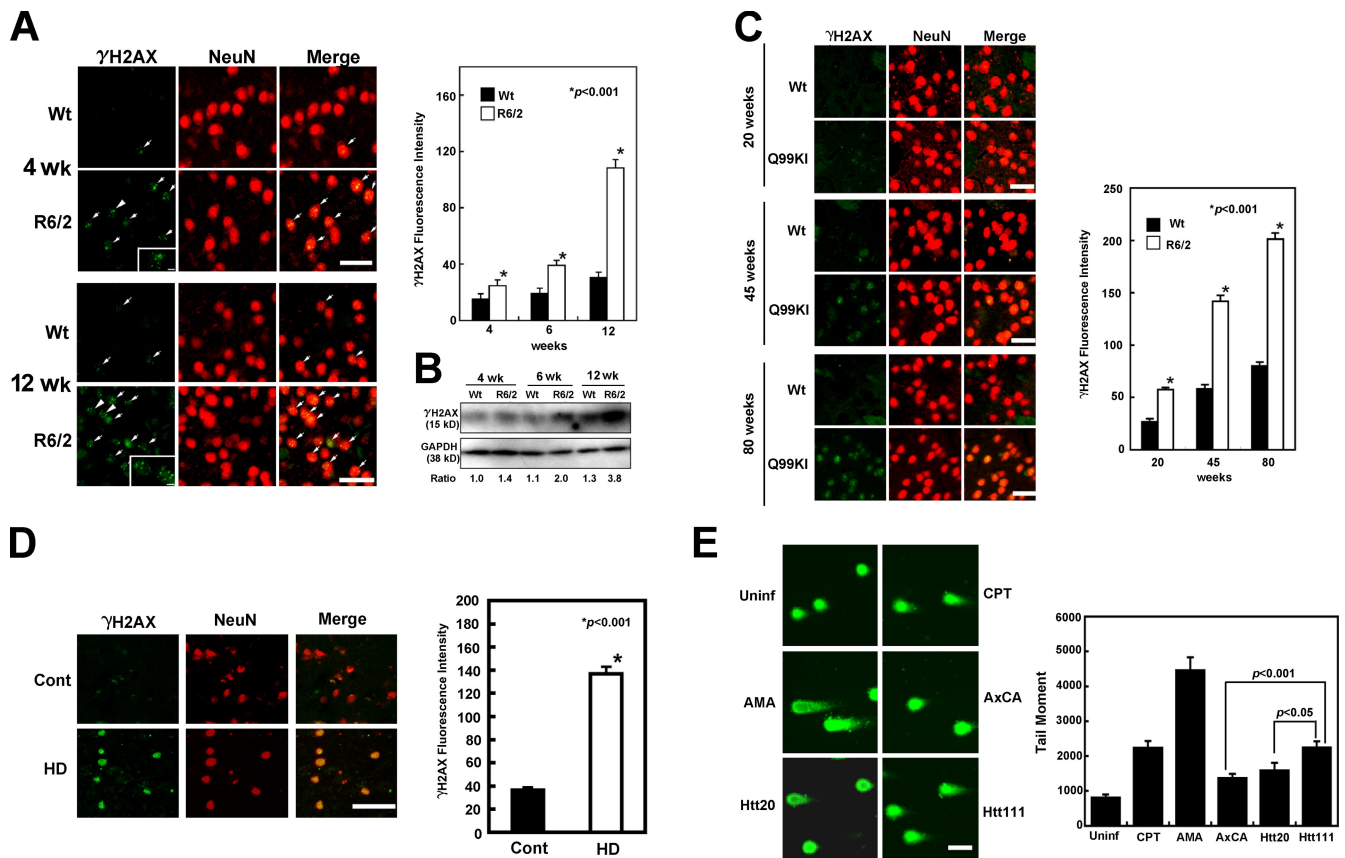


Figure 1. Accumulation of DNA DSBs in HD brains. (A, left) Immunohistochemical detection of γ H2AX (green) and NeuN (red) in the striatum of R6/2 and nontransgenic littermate (wt) mice at 4 and 12 wk of age. The γ H2AX signals were also merged with DAPI (Fig. S1). Arrows indicate activation of γ H2AX. Insets show higher magnification views of neurons indicated with arrowheads. (right) Immunofluorescence signal intensity of γ H2AX was quantified in >100 striatum neurons in nontransgenic littermates or R6/2 mice at 4, 6, and 12 wk of age. Student's *t* test indicated a significant difference of γ H2AX levels between wild-type and R6/2 mouse brains at each age. Bars, 25 μ m. (B) Immunoblot detection of γ H2AX level in wild-type and R6/2 mouse striatum protein extract (5 μ l) at 4, 6, and 12 wk of age shows that γ H2AX was activated in R6/2 mice. (C) Immunohistochemical detection of γ H2AX (green) and NeuN (red) in the striatum of HttQ99 knock-in (Q99KI) and nontransgenic littermate (wild type) mice at 20, 45, and 80 wk of age. (right) Immunofluorescence signal intensity of γ H2AX was quantified in >100 striatal neurons in normal littermate (wild type) and HttQ99 knock-in (Q99KI) mice. Bar, 25 μ m. (D) Striatal neurons of human HD patients show a remarkable increase of γ H2AX. The signal intensities of γ H2AX were analyzed in >100 neurons of three HD patients and of three nonneurological disease controls. Bar, 50 μ m. (E) Detection of mutant Htt-induced DNA DSBs by the neutral single-cell gel electrophoresis (comet assay). (left) Representative comet images of uninfected (Uninf), 10 μ g/ml CPT-treated, 20 μ g/ml α -amanitin-treated (AMA), AxCa empty virus-infected (AxCa), or AxCaHtt111Q-infected (Htt111Q) neurons at 4 d. Bar, 10 μ m. (right) Semiquantitative analysis of the results expressed as tail moment. Student's *t* test analysis demonstrated a significant difference in tail moments between neurons infected by AxCa and those by Htt111Q. *, *P* < 0.001. Error bars indicate SEM.

Hoshino et al., 2006). The genotoxic stress hypothesis seems consistent with previous notions that nuclear events initiate the polyQ disease pathology (Klement et al., 1998; Saudou et al., 1998; Katsuno et al., 2003). Moreover, regarding cell death, activation of p53–p73 pathway leads to apoptosis in cultured cells (Bae et al., 2005) and to nonapoptotic, atypical cell death in primary neurons (Hoshino et al., 2006).

There has been previous evidence for accumulation of DNA damage in HD. Kovtun et al. (2007) demonstrated that accumulated oxidative DNA damage triggers activation of a single base excision repair enzyme OGG1 that enhances the CAG repeat instability during aging in somatic cells of polyQ diseases. Our group showed that two polyQ disease proteins (HD and SCA1) interact and reduce high mobility group protein B proteins (Qi et al., 2007) essential for the repair of DNA double-strand breaks (DSBs) occurring naturally in transcription (Travers, 2003; Bianchi and Agresti, 2005; Ju et al., 2006).

Involvement of OGG1 indicates existence of base damages, whereas our results of H2AX phosphorylation (γ H2AX) suggest existence of DSBs in the polyQ pathology (Qi et al., 2007). Therefore, these two studies suggest that different types of DNA damage are induced in polyQ diseases.

The former study suggested that repair activity for oxidative DNA damage was not changed in nonneurological tissues from a mild HD mouse model, R6/1 (Kovtun et al., 2007), whereas our data suggested a reduction of DSB repair activity in vivo in neurons of *Drosophila melanogaster* and severe mouse models of HD (Qi et al., 2007). Another study implicating polyQ-induced DNA damage showed phosphorylation of H2AX in PC12 cells expressing expanded polyQ proteins as well as in fibroblasts from HD and SCA2 patients (Giuliano et al., 2003). Altogether, the questions remain of whether genomic double-strand DNA is actually cleaved especially in neurons, whether DNA repair is affected in polyQ diseases, and which molecules mediate the DNA repair dysfunction.

Addressing these questions, we found that mutant Htt interacts with Ku70, functionally impairs Ku70-dependent DNA-dependent protein kinase (DNA-PK) activity for nonhomologous end joining (NHEJ) of DSBs *in vitro* and *in vivo*, and contributes to the accumulation of DNA damage in neurons. Supplementation of Ku70 rescues mutant Htt-induced neurodegeneration in the R6/2 HD mouse model. These results suggest that impairment of DNA damage repair caused by the interaction between Ku70 and mutant Htt is a critical pathological component of HD.

Results

Mutant Htt induces DSBs of genomic DNA in neurons

In this study, we first addressed whether mutant Htt protein induces DSBs *in vivo* by analyzing R6/2 transgenic HD mice, expressing a polyQ-containing N-terminal Htt protein (Mangiarini et al., 1996). As a specific marker for DSBs, the levels of phosphorylated H2AX (γ H2AX) protein were investigated in neurons using fluorescence microscopy (Fig. 1). In our previous study, we showed that mutant Htt111Q protein expression increased γ H2AX levels in primary neurons (Qi et al., 2007). In immunohistochemistry experiments, we consistently found high signals of γ H2AX foci in striatal neurons of R6/2 mice (Fig. 1 A) that are located in the nuclei (Fig. S1 A). Correspondingly, γ H2AX was increased in Western blot analysis (Fig. 1 B). DSBs were similarly detected by 53BP1, a marker molecule of DNA damage focusing at DSB points (Schultz et al., 2000), whereas activation of Rad51, another DNA damage marker reflecting homologous recombination (Lieber et al., 2003), was not observed (Fig. S1 B). In positive controls of irradiated mouse brain tissues, 53BP1 but not Rad51 was activated (Fig. S1 C). The discrepancy between 53BP1 and Rad51 was consistent with the observation that homologous end joining is used in dividing neural stem/progenitor cells, but NHEJ is the major DNA repair system in postmitotic neurons (Orii et al., 2006). The foci of γ H2AX and 53BP1 were merged (Fig. S1 D). In R6/2 mice, γ H2AX was already increased at 4 wk of age, corresponding to the onset of symptoms in this mouse model (Fig. 1, A and B), which suggests that DSBs are an early event in HD pathogenesis. Interestingly, γ H2AX increased moderately in normal and transgenic mice during aging (Fig. 1, A and B), whereas the γ H2AX levels were significantly higher in R6/2 mice than in wild-type mice (Fig. 1, A and B).

We performed similar analyses with mutant Htt99Q knock-in mice (Q99KI) whose disease onset is \sim 45 wk (Ishiguro et al., 2001; Sawada et al., 2007) and with postmortem human HD patient brains. In striatal neurons of Q99KI mice, H2AX was also activated before disease onset and increased during aging (Fig. 1 C). Furthermore, striatal neurons in the human HD brains also showed high signals of γ H2AX in contrast to the nonneurological disease controls (Fig. 1 D).

To confirm the occurrence of mutant Htt-induced DSBs further, we directly analyzed cleavage of genomic DNA using the comet assay (Fairbairn et al., 1995; Olive and Banáth, 2006). The assay was performed with rat primary cortical neurons expressing mutant Htt111Q by adenovirus vector at 3 d

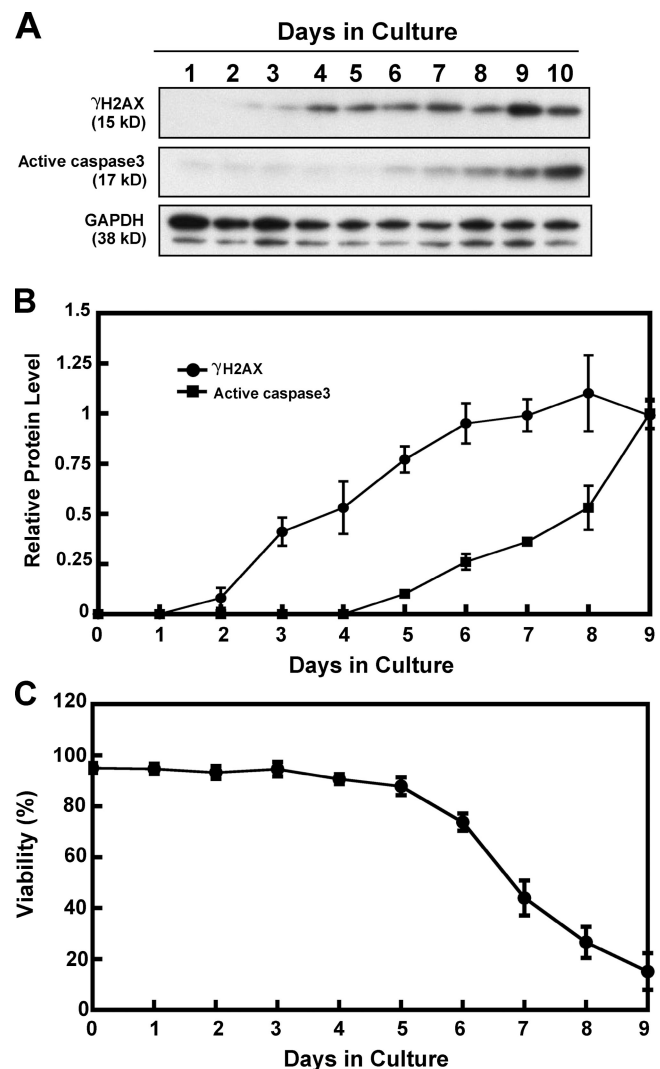


Figure 2. DNA damage precedes cell death. Chronological relationship among γ H2AX, caspase-3 activation, and viability of AxCaHtt111Q-infected primary cortical neurons. Caspase-3 activation was detected with anti-activated caspase-3 antibody that detects only the cleaved form of caspase-3. Activation of γ H2AX started at day 2 and preceded that of caspase-3 and cell death after day 5. Viability of neurons was evaluated by trypan blue staining. (A) Representative Western blots. (B) Quantitative analysis of signal intensities of γ H2AX and active caspase-3 and their chronological relationship. (C) Viability of primary cortical neurons expressing mutant Htt was estimated by trypan blue. Together with A–C, H2AX phosphorylation clearly precedes caspase-3 activation and cell death. Error bars indicate SEM.

after infection (Tagawa et al., 2004). Using neutral pH prevents denaturing of double-strand DNA to detect DSBs but not single-strand breaks (SSBs) reported previously (Illuzzi et al., 2009). Camptothecin (CPT), a specific inhibitor of DNA topoisomerase I (TopI), increased tail moment in the comet assay, indicating DSBs as a positive control (Fig. 1 E). As expected, expression of mutant Htt (Htt111Q) in cortical neurons similarly induced DSBs (Fig. 1 E). The difference from normal Htt (Htt20Q) was statistically significant (Fig. 1 E). Interestingly, α -amanitin, a specific inhibitor of RNA polymerase II, also induced a substantial increase of DSBs (Fig. 1 E), agreeing with the recent notion that transcription is coupled with DNA repair

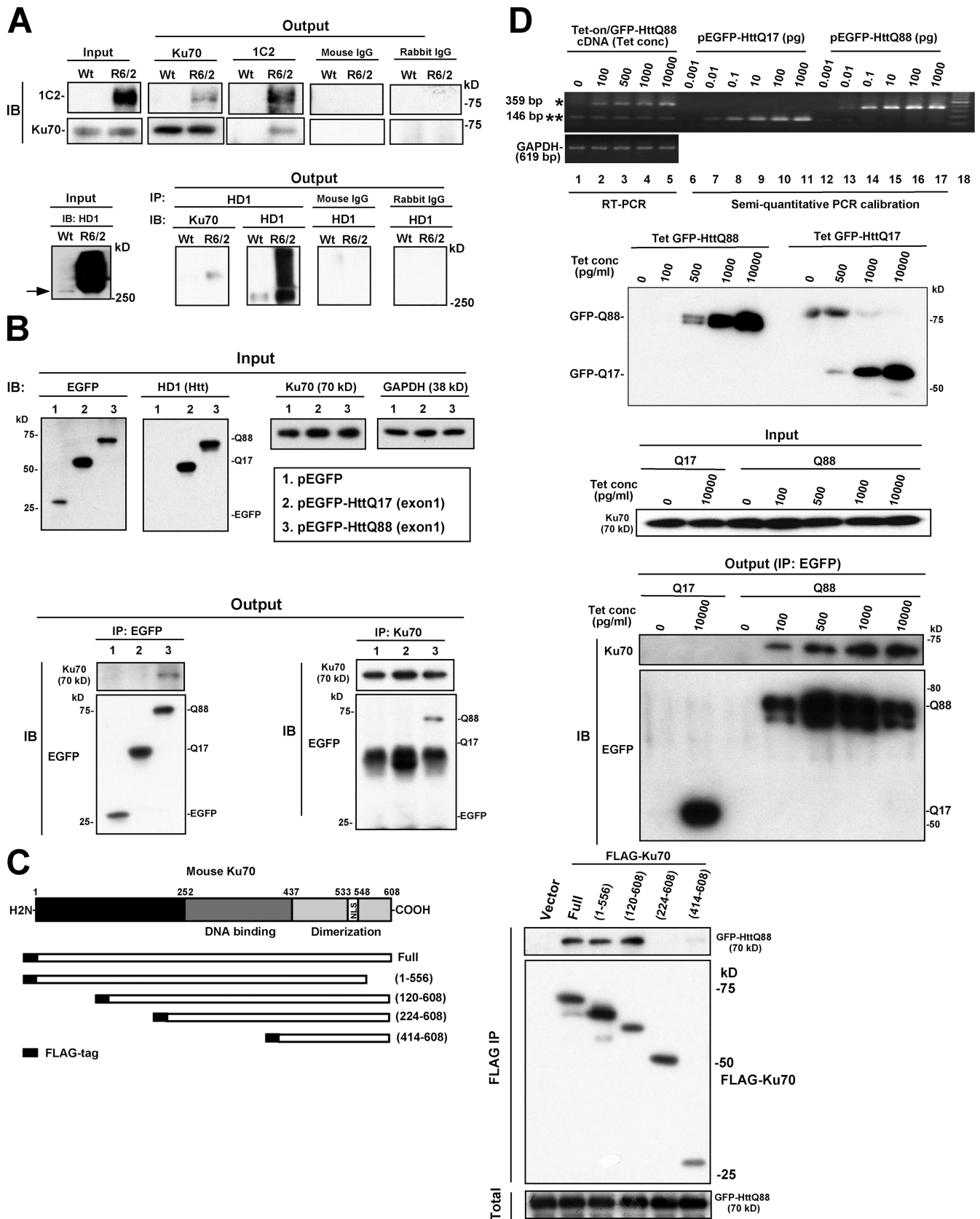


Figure 3. **Protein-protein interaction between Ku70 and mutant Htt.** (A) IP assay with mouse brain samples. The nuclear extract from brain samples (cerebral cortex and striatum) of R6/2 or nontransgenic littermate (wt) mice at 9 wk were precipitated with anti-Ku70, -1C2, or -HD1 antibody and blotted with the other antibody. In the case of HD1 antibody, wild-type full-length Htt and aggregation of mutant Htt at the gel top are shown in input (arrow). In output, only the mutant Htt was coprecipitated with Ku70. As negative controls, mouse and rabbit IgG were used for precipitation. (B) IP assay showing interaction between endogenous Ku70 and overexpressed mutant Htt88Q exon 1 in HeLa cells. Interaction between normal Htt and endogenous Ku70 was not clear

(Ju et al., 2006) and our previous finding that impairment of transcription induces genotoxicity (Qi et al., 2007).

DNA damage occurs before apoptotic signal activation

To know whether DNA damage could be causative for cell death, we analyzed the chronological relationship between H2AX phosphorylation, caspase-3 activation, and cell death in Htt111Q-expressing primary cortical neurons (Fig. 2). The emergence of γ H2AX was observed at day 2 and clearly preceded the cleavage of caspase-3 that started at day 5 (Fig. 2). Cell death detected by trypan blue initiated at day 6 after caspase-3 activation. These results suggest that DNA damage indicated by γ H2AX activation is not the result of cell death and that the DSBs detected by comet assay (Fig. 1 E) could be an upstream event for mutant Htt-induced neuronal death.

Ku70 interacts with mutant Htt

An interactome dataset of Htt by Goehler et al. (2004) included a molecule relevant to DSB repair, Ku70, which was not identified in our previous proteome or transcriptome approaches (Qi et al., 2007; Tagawa et al., 2007). Ku70 plays a critical role in DSB repair (Lombard et al., 2005; for review see Sancar et al., 2004). It forms a protein complex with Ku80, recruits DNA-PK catalytic subunit (DNA-PKcs; p460) complex to the DNA ends, and activates XRCC4/DNA ligase IV (for review see Sancar et al., 2004). Ku70 by itself does not have the enzymatic activity for NHEJ of DSBs, whereas it is indispensable for the formation and kinase activity of the ternary complex composed of Ku70, Ku80, and DNA-PKcs (Lombard et al., 2005). Therefore, mutant Htt might impair NHEJ of DSBs by the DNA-PK complex through interaction with Ku70.

To test this hypothesis, we examined the interaction between Ku70 and full-length mutant Htt in HEK293 cells by immunoprecipitation (IP; Fig. S2 A). The interaction was detected either by Ku70 or Htt precipitation (Fig. S2 A). Next, we confirmed the interaction between the mutant Htt exon 1 peptide and endogenous Ku70 by IP with R6/2 mouse brain (cerebral cortex and striatum) tissues (Fig. 3 A). Although coprecipitation of Ku70 and mutant Htt was observed with anti-polyQ and -Htt antibodies (1C2 and HD1), an interaction with wild-type Htt was not detected. In IPs with HeLa cells, an interaction of Ku70 with wild-type Htt could also not be shown (Fig. 3 B). We reexamined the interaction with wild-type Htt exon 1 using the LUMIER assay (luminescence-based mammalian interactome

mapping technology; Barrios-Rodiles et al., 2005). When Ku70 and wild-type Htt were overexpressed in the assay, their interaction was observed with low stringency (Fig. S2 B). These data collectively suggest that the shorter Htt exon 1 peptides, including the polyQ tract, do interact with Ku70 and that mutant Htt interacts with Ku70 more strongly than wild-type Htt. We also found that mutant Htt did not interact with Ku80 or DNA-PKcs in IP (unpublished data).

We also performed IP with deletion clones of Ku70 to determine the interaction domain for mutant Htt (Fig. 3 C). Ku70 is composed of three domains (Fig. 3 C, top): the N-terminal domain, the DNA-binding domain, and the dimerization domain (Byrum et al. 2004). The interaction was observed with the construct 120–608 but not with 224–608, indicating that the mutant Htt exon 1 peptide interacts with the 120–223 region of the N-terminal domain. Functions of the N-terminal domain are not known in detail, whereas its deletion profoundly impairs DNA-PK activity, DNA repair after ionizing radiation, and DNA end binding of Ku70 (Jin and Weaver, 1997).

Furthermore, we titrated the amount of mutant Htt necessary for the interaction with Ku70 by using stable T-Rex-HeLa cells in which expression levels of mutant Htt can be controlled by the concentration of tetracyclin in the culture medium. RT-PCR was used to compare endogenous wild-type Htt and Tet-induced mutant Htt (Fig. 3 D, top). Induced wild-type and mutant Htt proteins were also checked by Western blots (Fig. 3 D, middle). Simultaneously, coprecipitation of Ku70 with Htt was tested. We found that an expression level of mutant Htt almost equivalent to the expression level of endogenous Htt was sufficient for interaction with Ku70 (Fig. 3 D, bottom). A nonspecific band \sim 75 kD interacting with anti-GFP antibody was observed in TetGFP-Htt17 cells. The nonspecific bands decreased in a tetracyclin concentration-dependent manner as a result of an unknown reason.

Immunocytochemistry of primary cortical neurons expressing mutant Htt also supported the association between Htt and Ku70 because mutant Htt and Ku70 were colocalized in inclusion bodies of primary cortical neurons (Fig. 4 A). Mutant Htt and Ku70 were also colocalized in striatal neurons of R6/2 mice (Fig. 4 B). Higher magnification and confocal microscopic analyses revealed colocalization of Ku70 and mutant Htt both in inclusion bodies and the nucleoplasm (Fig. 4 C). Quantitative analysis of the signal intensities in the nucleus revealed that Ku70 distribution was strongly associated with that of mutant Htt, whereas ordinary distribution of Ku70 was homogenous

in this condition. (C) Deletion analysis demonstrated that mutant Htt interacts with the N-terminal domain of Ku70. (top) Diagram shows the constructs for the deletion analysis. (bottom) Coprecipitation pattern of GFP-HttQ88 with various Flag-Ku70 deletion mutants. NLS, nuclear localization signal. (D) The amount of mutant Htt necessary for interaction with endogenous Ku70 was titrated with Tet-on stable cells in which mutant Htt expression can be regulated by the concentration of tetracyclin in the medium. (top) Lanes 1–5 indicate a semiquantitative RT-PCR experiment with Htt-specific primers using cDNAs obtained from the Tet-on EGFP-HttQ88 stable cells treated with tetracyclin at different concentrations (0–100,000 pg/ml) for 48 h. The Htt-specific primers are designed to amplify the CAG repeat region to distinguish the endogenous Htt and induced EGFP-HttQ88 genes. The single asterisk denotes induced GFP-HttQ88 transcripts, the double asterisk denotes endogenous Htt transcripts (lanes 1–5). As a control, corresponding PCR with GAPDH-specific primers was performed. As a semiquantitative PCR calibration, PCR was performed with the Htt primers using plasmid DNAs, pEGFP-HttQ17 (lanes 6–11), and pEGFP-HttQ88 (lanes 12–17) as PCR templates with indicated amounts to evaluate the RT-PCR. (middle) Equal amounts of cell lysate from the Tet-on stable cell lines treated with the indicated concentration of tetracyclin for 48 h were blotted with anti-GFP antibody. (bottom) The lysates were also subjected to IP with anti-GFP antibody, and the precipitants were blotted with anti-Ku70 and GFP antibodies. IB, immunoblot.

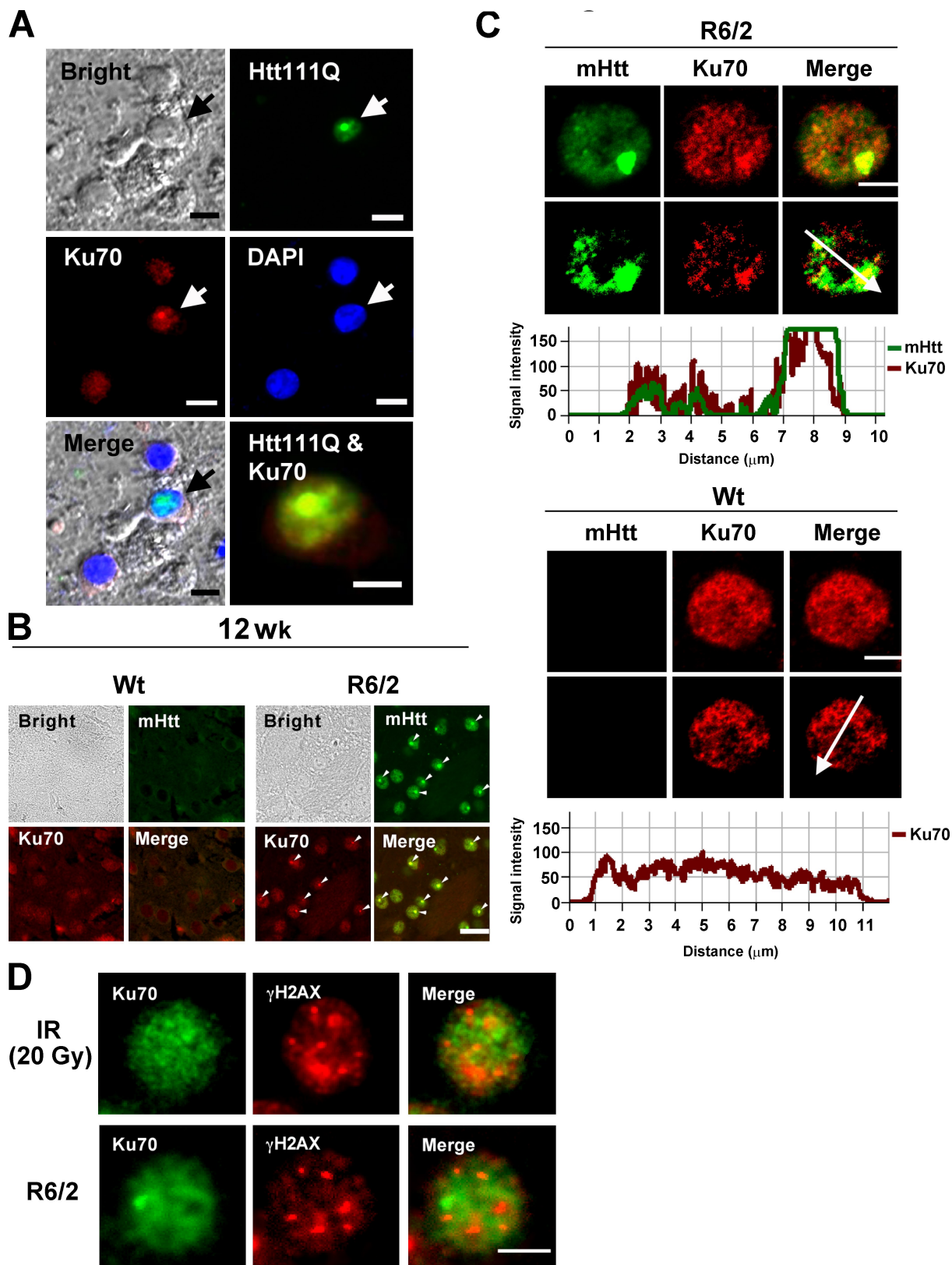


Figure 4. **Colocalization of Ku70 and mutant Htt in the nucleus.** (A) Immunocytochemical detection of colocalization of Ku70 and mutant Htt in cultured neurons at 4 d after mutant Htt infection (arrows). Endogenous Ku70 (red) colocalized with mutant Htt inclusion (green) in cultured neurons infected by AXCA-Htt111Q. Bars, 5 μm . (B) Immunohistochemical analysis showing colocalization of endogenous Ku70 (red) and mutant Htt (green) in striatal neurons of R6/2 mice (arrowheads) and age-matched nontransgenic littermates (wild type [wt]) at 12 wk. Bar, 25 μm . (C) High power magnification of striatal neurons of R6/2 mice and nontransgenic littermates (wild type) at 12 wk. Top and middle show ordinary and confocal microscopic images, respectively. (bottom) Graphs show quantitative analyses of signal intensities acquired from confocal images along the arrow line, showing that Ku70 and mutant Htt are colocalized. Bars, 5 μm . (D) γH2AX is not colocalized with Ku70. IR, wild-type mouse brain irradiated with 20 Gy. Bar, 5 μm .

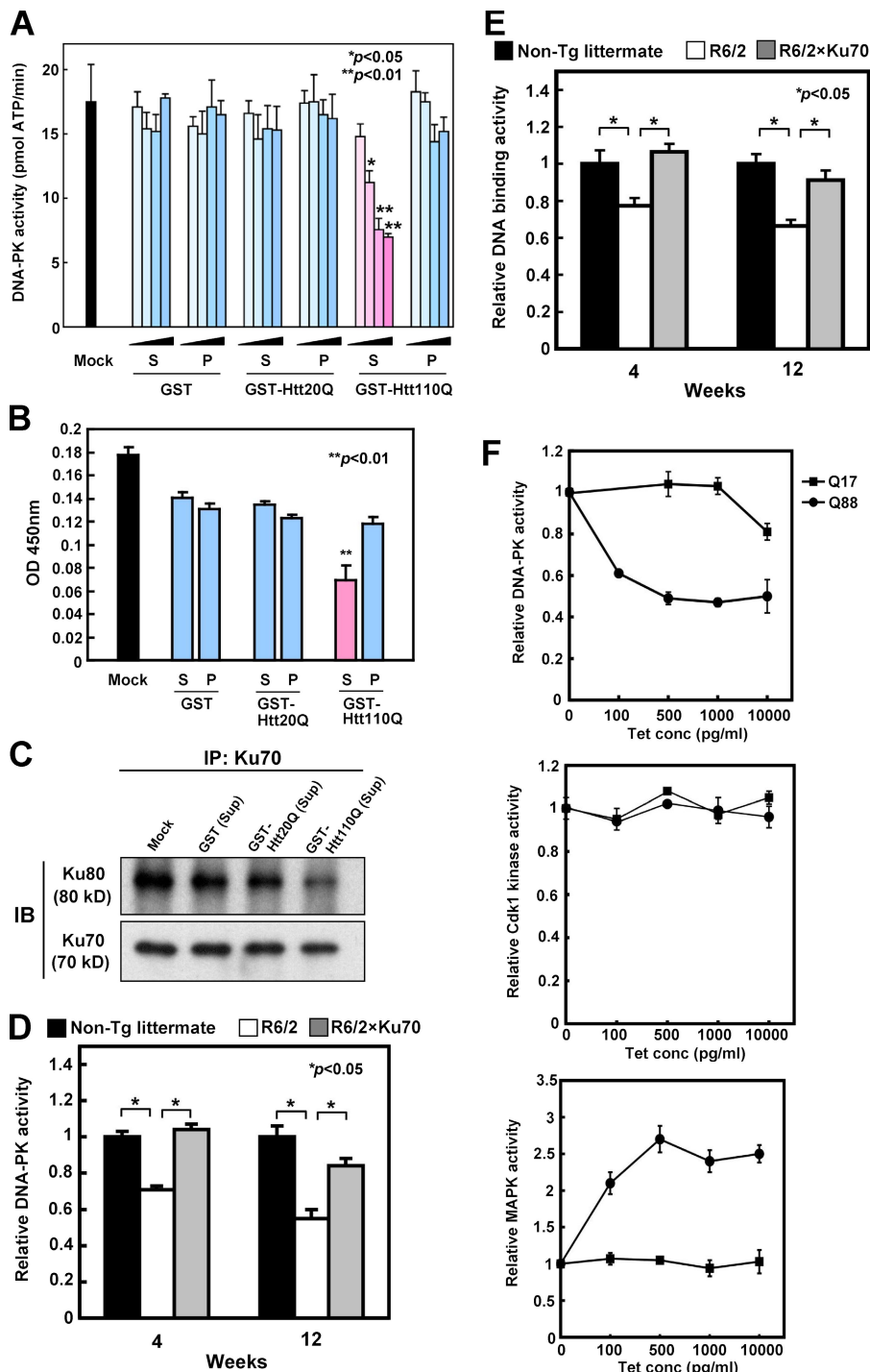


Figure 5. Mutant Htt affects DNA-PK activity and DNA-PK complex formation in vitro and in vivo. (A) The effect of soluble/insoluble fractions of wild-type Htt (GST-Htt20Q) or mutant Htt (GST-Htt110Q) on the DNA-PK activity was examined with HeLa cell nuclear extract. Addition of the supernatant fraction (S) but not the pellet fraction (P) of mutant Htt suppressed DNA-PK activity in a dose-dependent manner (mean \pm SD; $n = 3$). Normal Htt or GST proteins did not affect DNA-PK activity. Student's *t* test confirmed the difference between GST and GST-Htt110Q. The gradient indicates that 5, 15, 50, or 150 ng of each fraction was added to 25 μ l of reaction. (B) Ku70 binding to DNA was assayed as described in Materials and methods. Supernatant of GST-Htt110Q suppressed binding of Ku70 to the cleaved DNA fragments attached to the bottom of dishes. (C) IP was performed with the samples used for DNA-PK activity assay. GST-Htt110Q supernatant impaired DNA-dependent Ku70-Ku80 complex formation. (D) DNA-PK activity was assayed with nuclear extract from brain samples (cerebral cortex and striatum) of R6/2 or nontransgenic littermate (wild type) mice. Mean \pm SD ($n = 4$) are shown. Relative activities were calculated as the ratio to the mean value of wild-type mice. Corresponding data of R6/2; Ku70 double-transgenic mice are also shown. (E) Ku70 binding to DNA was assayed with nuclear extract from brain samples of R6/2 or nontransgenic littermate (wild type) mice. Mean \pm SD; $n = 3$. Data of R6/2; Ku70 double-transgenic mice are also shown. (F) DNA-PK, Cdk1, and MAPK/ERK activities were assayed with the Tet-on EGFP-HttQ17 and EGFP-HttQ88 stable cell lines in which induced levels of EGFP-Htt can be regulated by the concentration of tetracycline. The amount of mutant Htt necessary for impairing DNA-PK activity was titrated. Nuclear extracts from the Tet-on GFP-HttQ17 and GFP-HttQ88 stable cell lines treated with the indicated concentration of tetracyclin for 48 h were subjected to the DNA-PK assay. The induction levels of GFP-HttQ17 and GFP-HttQ88 were similar to Fig. 3 D because the two experiments were performed simultaneously. (top) An amount of mutant Htt equivalent to the endogenous Htt expression level was sufficient for inhibition of DNA-PK activity. (bottom) Meanwhile, mutant Htt did not inhibit Cdk1 and MAPK/ERK activities. These results indicated that inhibition of DNA-PK was specific. Error bars indicate SEM.

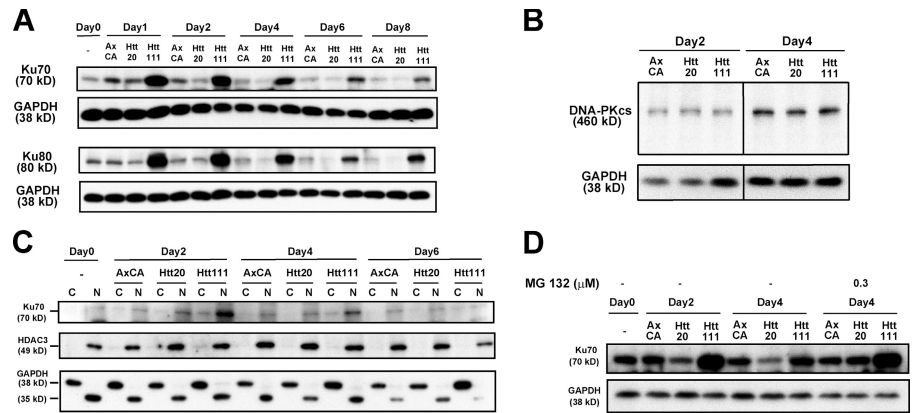
and not remarkably altered (Fig. 4 C). However, the foci of γ H2AX-indicating DSBs were distributed outside of the inclusion bodies containing Ku70 and mutant Htt (Fig. 4 D).

Interaction between mutant Htt and Ku70 impairs DNA repair function of the DNA-PK complex

Next, we examined the effect of mutant Htt on DNA-PK activity. We prepared GST and GST mutant Htt (Htt110Q) fusion proteins (Fig. S3 A), added them into the nuclear extract of HeLa cells containing Ku70, Ku80, and DNA-PKcs, and assayed

the DNA-PK activity (Fig. 5). We found that GST-Htt110Q (exon 1) but not GST or GST-Htt20Q protein suppressed DNA-PK activity (Fig. 5, A and B; and Fig. S3 B). Interestingly, the suppression occurred only in the soluble fraction but not in the insoluble fraction of mutant Htt protein (Fig. 5 A). Soluble GST-Htt110Q also impaired Ku70-DNA binding (Fig. 5 B) and affected Ku70-Ku80 interaction (Fig. 5 C), whereas GST-Htt20Q disturbed neither DNA-PK activity, Ku70-DNA binding, nor Ku70-Ku80 complex formation. Moreover, DNA-PK activity and Ku70-DNA interaction were impaired in the nuclear extract from brain tissues of R6/2

Figure 6. **Mutant Htt affects Ku70 and Ku80 expression in primary cortical neurons.** (A) By Western blotting, Ku70 and Ku80 expression in primary cortical neurons was investigated chronologically after infection of AxCa, AxCaHtt20Q, (Htt20Q), or AxCaHtt111Q (Htt111Q). (B) Mutant Htt does not affect expression of DNA-PKcs. Immunoblot detection of the change of DNA-PKcs expression in cultured neurons at 2 and 4 d after virus infection. Cultured neurons infected by AxCa, AxCaHtt20Q, (Htt20Q), or AxCaHtt111Q (Htt111Q) were collected, and the cell lysates (5 μ g) were immunoblotted by anti-DNA-PKcs (H-163) antibodies. (C) The chronological change of Ku70 expression in cytosol and nucleus in cultured neurons. 1 μ g nuclear (N) or cytosol (C) protein extract was blotted by anti-Ku70 antibody (H-308). Detection of GAPDH and HDAC3 was used to determine the purity of the fractions. Ku70 expression changed only in the nucleus. The lower GAPDH band in the nuclear fraction might be the nuclear translocation form (Sawa et al., 1997; Dastoor and Dreyer, 2001). (D) Effect of proteasome inhibitor on Ku70 protein levels in neurons was examined by immunoblots. Neurons infected by AxCa, AxCaHtt20Q (Htt20Q), or AxCaHtt111Q (Htt111Q) cultured in the presence or absence of proteasome inhibitor MG-132 were used for the analysis. 0.3 μ M MG-132 was added to the culture medium 2 d after virus infection (day 2). Neurons were collected after 2 d of treatment with or without MG-132 (day 4).



mice when compared with nontransgenic littermates (Fig. 5, D and E; and Fig. S3 C). Simultaneously, we observed that transgenic expression of Ku70 rescued the decrease of DNA-PK activity and Ku70–DNA interaction in R6/2 mice (Fig. 5, D and E), which will be discussed later. As mutant Htt interacts only with Ku70 among three components of the DNA-PK complex in IP assay (unpublished data), these results collectively suggest that the soluble form of mutant Htt directly disturbs the DNA-PK complex function through interaction with Ku70, which is consistent with the recent concept that soluble mutant Htt is toxic (Arrasate et al., 2004).

Furthermore, by using the T-Rex–HeLa cell system described in Fig. 3 D, we titrated the amount of mutant Htt necessary for inhibition of DNA-PK activity (Fig. 5 F). Expression levels of mutant and wild-type Htt-EGFP can be controlled via the tetracyclin concentration (Fig. 3 D). We found that an amount of mutant Htt almost equivalent to the endogenous Htt expression level was sufficient for inhibition of DNA-PK activity (Fig. 5 F). These results (Fig. 3 D and Fig. 5 F) support that mutant Htt expressed in human patients could impair Ku70-mediated DNA damage repair. Meanwhile, mutant Htt expression did not suppress activities of other kinases such as Cdk1/Cdc2 or MAPK/extracellular-regulated kinase (ERK; Fig. 5 F), supporting the view that the effect of mutant Htt on DNA-PK could be specific to some extent. In yeast cells, Cdk1 is known to be essential for DNA damage checkpoint activation (Ira et al., 2004). MAPK/ERK is known to be activated in the striatum of R6/2 mice, although a downstream kinase MSK1 is inactivated (Roze et al., 2008).

Mutant Htt induces Ku70 expression

In addition to the direct inhibition of DNA-PK activity through binding to Ku70, mutant Htt might influence expression levels of Ku70 or of other components in the DNA-PK complex. Therefore, we tested how Ku70, Ku80, and DNA-PKcs respond to mutant Htt expression. Western blot analysis with primary cortical neurons expressing mutant Htt showed that protein levels of Ku70 and Ku80 but not of DNA-PKcs transiently

increased at day 1, decreased from day 1 to day 6 after infection, and returned to the initial level (Fig. 6, A–C). The early up-regulation of Ku70 and Ku80 probably occurs as a secondary response to DNA damage (Browne et al., 1999) induced by oxidative damage and by impaired DNA-PK activity as a result of an interaction between Ku70 and mutant Htt (Fig. 4 A). The decrease of Ku70 was blocked by the protease inhibitor MG132 (Fig. 6 D), indicating that one part of the Ku70 and mutant Htt complex was degraded by the proteasome system, whereas another part forms intracellular aggregates.

In R6/2 mice from 4 to 12 wk, the amount of Ku70 protein was stable. This suggests that, after a short-term transient fluctuation at the embryonic stage, the Ku70 protein expression level becomes stable at the equilibrium between increased synthesis and increased degradation of Ku70. It is of note that Ku70 signal levels in the nucleoplasm of inclusion-positive neurons were not reduced in vitro and in vivo (Fig. 4, A and B).

Ku70 is a bifunctional protein with different roles in the cytoplasm and nucleus. In the cytoplasm, Ku70 is suggested to associate with Bax to prevent apoptosis. Acetylation of Ku70 seems to inhibit the interaction with Bax and promote apoptosis (Cohen et al., 2004). However, acetylated Ku70 was not found in cortical neurons before or after expression of mutant Htt (unpublished data). Altogether, the functional defect of Ku70 seems to be directly induced by interaction with mutant Htt rather than indirectly by sequestration or acetylation of Ku70.

DNA damage by mutant Htt depends on the dose of nonbound Ku70

To test the specificity of mutant Htt-induced DSBs, we used a Tet-on double-expression system for DsRed and Htt103Q. We found that doxycycline-induced expression of mutant Htt directly triggered GFP-H2AX foci formation in HeLa cells (Fig. 7 A). Meanwhile, H2AX foci formation was not induced by doxycycline only in cells that did not express Htt103Q (Fig. 7 B, arrow) or in cells expressing only DsRed (Fig. 7, A and C). These results confirm that mutant Htt (but not transfection or doxycycline treatment) induces DSBs. The results

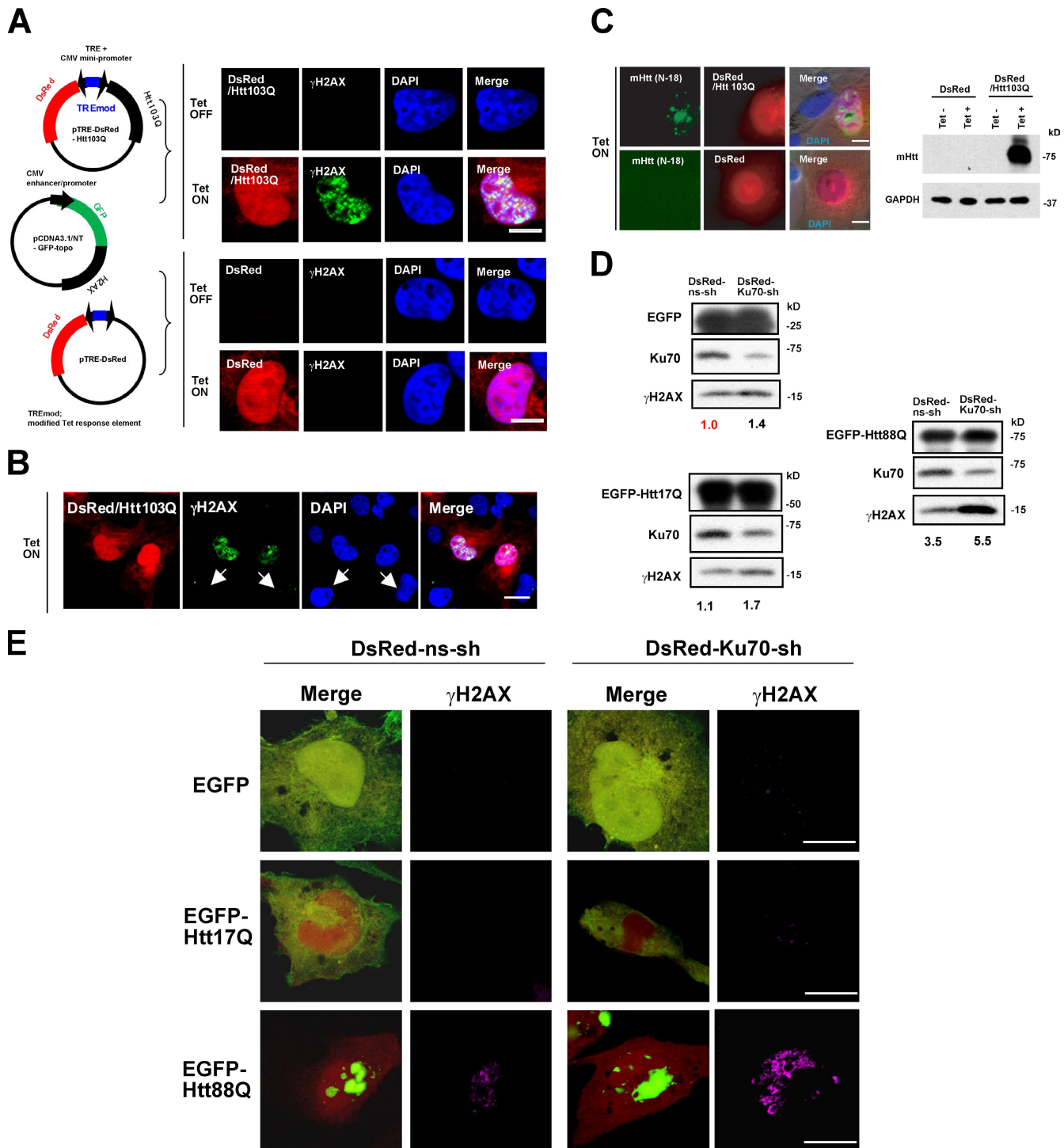
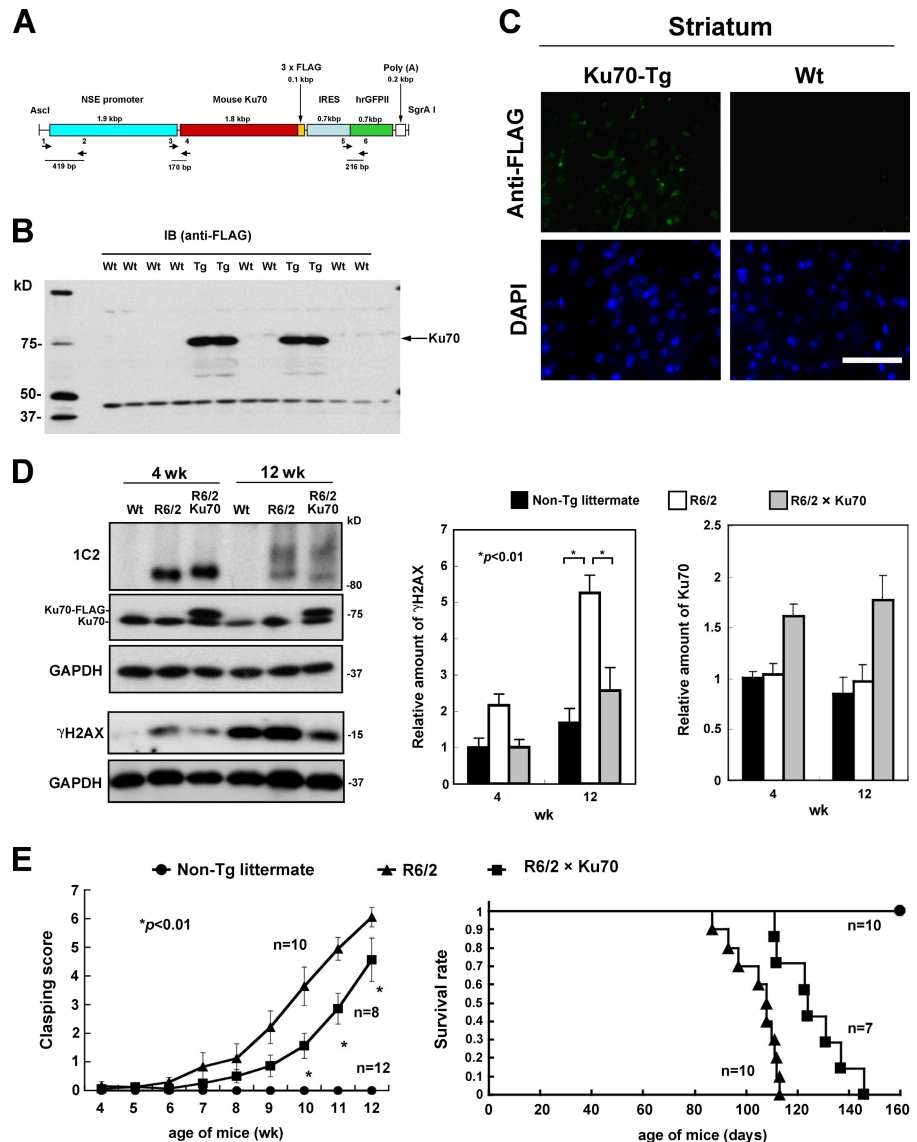


Figure 7. Mutant Htt specifically induces γ H2AX activation in a Ku70 dose-dependent manner. (A) After triple transfection of pTet-on, pTRE-DsRed-Htt103Q, and GFP-H2AX plasmids into HeLa cells, Htt expression was induced by addition of doxycycline; H2AX activation was detected by anti- γ H2AX antibody. The Htt103Q/DsRed-expressing cells showed foci formation of GFP-H2AX (Siino et al., 2002) only after induction. The cells expressing only DsRed did not show foci formation even after addition of doxycycline. CMV, cytomegalovirus. Bar, 5 μ m. (B) In the same field, doxycycline did not induce foci of γ H2AX in nontransfected cells (arrows). Bar, 10 μ m. (C) Immunocytochemistry (left) and Western blot analysis (right) show induction of Htt103Q by doxycycline. Bars, 5 μ m. (D) Suppression of Ku70-enhanced activation of γ H2AX. pDsRed-Ku70-shRNA and pEGFP-Htt88Q were cotransfected into HeLa cells, and immunoblots were performed with total cells. pDsRed-nonsilencing shRNA, pEGFP-Htt17Q, or pEGFP was used as control. Transfection rates of each plasmid were confirmed to be equivalent. Activation levels of H2AX (γ H2AX band signals) were corrected by the band intensities of EGFP or its fusion proteins in the same blot, and the value of DsRed-nonsilencing shRNA/EGFP was defined as 1.0. (E) Confocal microscopic analysis of immunocytochemistry of γ H2AX in DsRed/EGFP double-positive cells. DsRed-Ku70-shRNA-expressing cells showed higher signals of γ H2AX in comparison with control cells. Bars, 5 μ m.

Figure 8. Ku70 overexpression ameliorates mutant Htt-induced symptoms in mice. (A) The DNA fragment for generation of mouse Ku70 transgenic mice. Mouse Ku70 flanked to Flag and humanized recombinant GFP11 (Agilent Technologies) are driven by rat NSE enhancer/promoter, which is also active in mice. (B) Immunoblot (IB) detection of Ku70-Flag expression in mouse striatum by anti-Flag antibody. Wt, wild type (nontransgenic littermate). (C) Ku70-Flag expression was detected by anti-Flag antibody in immunohistochemistry in the Ku70 transgenic mouse brain. The expression of Ku70-Flag protein was detected in the striatal neurons of Ku70 transgenic mice by anti-Flag antibody. Nontransgenic littermate mice show nonspecific stains of small vessels but not those of neurons. Bar, 50 μ m. (D) In vivo effect of Ku70 overexpression on the γ H2AX level in the striatum was examined by Western blots at 4 and 12 wk. γ H2AX was suppressed in R6/2 \times Ku70 double-transgenic mice. Anti-Ku70 antibody detected both endogenous Ku70 and overexpressed Ku70-Flag. The mutant Htt bands at 12 wk were shifted upward in comparison with the bands at 4 wk, indicating aggregation of mutant Htt. In the double-transgenic mice, the band sizes of mutant Htt were always slightly different from those in R6/2, suggesting that Ku70 might unexpectedly influence the conformation or aggregation state of mutant Htt (1C2). (right) Quantitative analysis of the left blot is shown. γ H2AX band intensities were corrected by GAPDH. *, $P < 0.01$ by Student's t test. (E) Effect of neuron-specific Ku70 overexpression on lifespan was evaluated by Kaplan-Meier analysis. Nontransgenic littermate (\bullet), R6/2 transgenic mice (\blacktriangle), and R6/2 and Ku70 double-transgenic mice (\blacksquare) are shown. Lifespan elongation was significant at the end point in log-rank test ($P = 0.0007$). The evaluators of these experiments were blinded. The number of mice is shown as ($n = x$). Error bars indicate SEM.



therefore deny the possibility that toxicity of adenovirus infection causes DSBs.

We also tested whether additional reduction of Ku70 enhances DSBs when the expression level of mutant Htt is equivalent. We expressed mutant Htt labeled by EGFP in HeLa cells and repressed Ku70 by a coexpression vector of Ku70–short hairpin RNA (shRNA) and DsRed protein. We investigated DSBs by immunoblots with anti- γ H2AX antibody. As expected, reduction of Ku70 enhanced phosphorylation of H2AX (Fig. 7 D). Immunocytochemistry of EGFP/DsRed double-positive cells with confocal microscopy supported the result of immunoblots (Fig. 7 E).

We also tried to test the effect of Ku70 reduction on mutant Htt-induced neurodegeneration in vivo by generating Ku70^{-/-}; mutant Htt^{+/-} mice from Ku70^{-/-} mice (Gu et al., 2000). However, Ku70^{-/-} mice were infertile in a separate experiment (unpublished data). Instead, we generated double-heterozygous mice (Ku70^{+/-}; mutant Htt^{+/-}), some of which showed more severe symptoms than R6/2 mice, although the difference was not confirmed statistically (unpublished data). However, in these double-heterozygous mice, Ku70 and DNA-PK activity were

not significantly reduced in comparison with the wild-type mice (unpublished data). Therefore, we could not determine whether a further reduction of Ku70 accelerates mutant Htt-induced neurodegeneration at the mouse level.

Supplementation of Ku70 rescues neurodegeneration in mice

We next asked whether functional recovery of Ku70 by increasing the amount of Ku70 rescues neurodegeneration in vivo. We hypothesized that additional overexpression of Ku70 would change the equilibrium between mutant Htt and Ku70 and would increase the amount of free and functional Ku70 (nonbound to mutant Htt). We generated transgenic mice overexpressing Ku70-Flag protein under the control of the neuron-specific enolase (NSE) enhancer/promoter (Fig. 8 A). The expression of Ku70-Flag protein was detected in the striatum of transgenic mice by Western blot analysis (Fig. 8 B) and immunohistochemistry (Fig. 8 C). Expression from the Ku70 transgene was also detected in neurons throughout the brain, including cerebral cortex and hippocampus (Fig. S4 A). Macroscopic and phenotypic

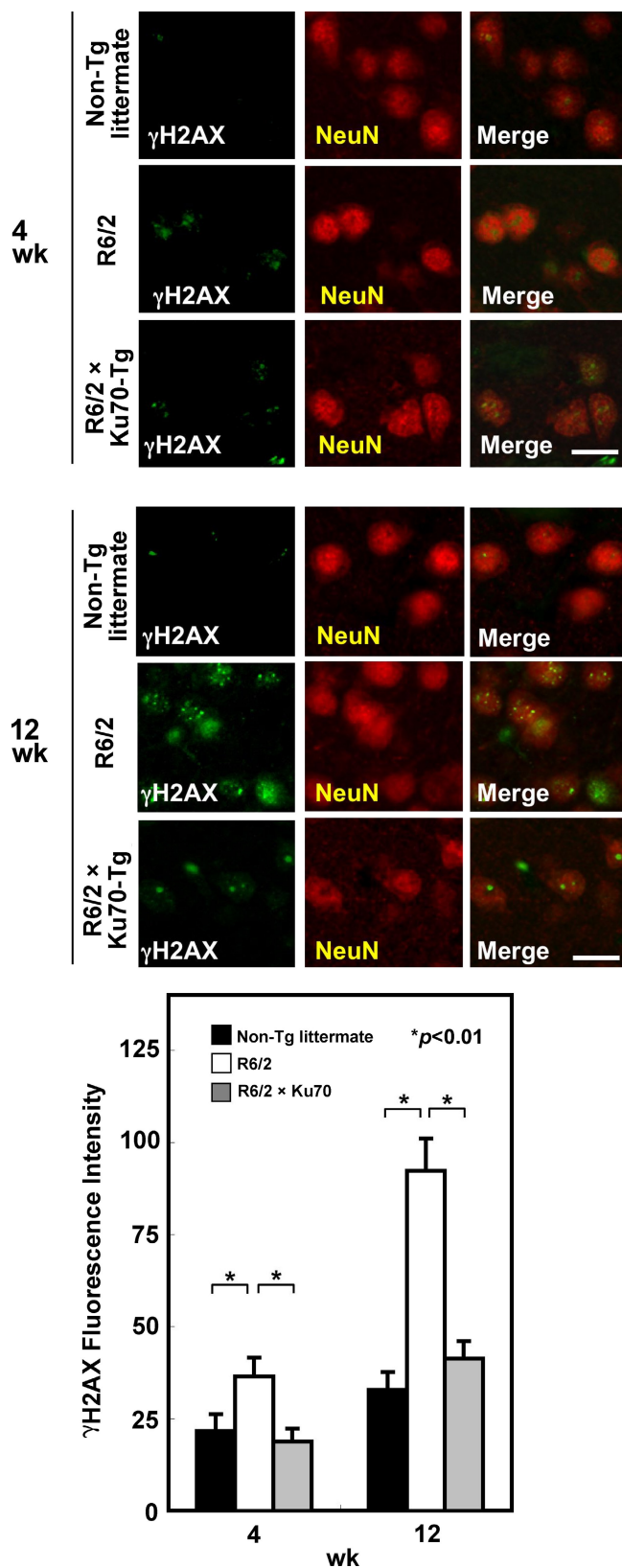


Figure 9. Ku70 overexpression ameliorates mutant Htt-induced activation of H2AX in mouse striatal neurons in vivo. Immunohistochemistry of striatal neurons of R6/2 mice or of R6/2 x Ku70 double-transgenic mice at 4 wk. Anti-NeuN and γ H2AX antibodies were used. Bars, 10 μ m. (bottom) Quantitative analysis of >100 neurons from four nontransgenic littermates, four R6/2, and four double-transgenic mice is shown. The

analysis showed no abnormality in Ku70 transgenic mice, and the birth rate was normal (unpublished data).

We crossed the Ku70 transgenic mice with R6/2 mice and generated double-transgenic mice. Western blot analysis showed Ku70-Flag expression in addition to endogenous Ku70 in double-transgenic mice (Fig. 8 D). As expected, overexpression of Ku70 decreased γ H2AX at 4 and 12 wk, and the reduction was statistically confirmed (Fig. 8 D). We analyzed lifespan, brain weight, body weight, and motor functions of the double-transgenic mice (Fig. 8 E and Fig. S4 B). The abnormal clasping reflex was significantly reduced in double-transgenic mice until 12 wk ($P < 0.01$; Fig. 7 E). Lifespan was also significantly improved (log-rank test; $P = 0.0007$; Fig. 8 E). Rotarod staying time of double-transgenic mice was slightly improved at 4 wk (before onset) in comparison with R6/2 mice ($P < 0.05$), whereas the difference disappeared over time (Fig. S4 A). Brain weight was slightly improved at 4.5 wk (Fig. S4 A).

We further investigated histological changes of the double-transgenic mice (Fig. 9 and Fig. S4 C). Consistent with Western blot analysis (Fig. 8 D), immunohistochemistry showed lower γ H2AX signals in the double-transgenic mice than in R6/2 mice at 4 and 12 wk (Fig. 9). We found a unique change of the γ H2AX intranuclear distribution in striatal neurons of the double-transgenic mice. γ H2AX was concentrated to fewer dots (Fig. 9) that were not merged with inclusion bodies of mutant Htt (Fig. S4 C) but costained with a nucleolus marker, fibrillarin (Fig. S5). Similar patterns were also observed in wild-type littermates (Fig. 9). The signals of γ H2AX in the nucleoplasm were clearly reduced in the double-transgenic mice in comparison with R6/2 mice (Fig. 9 and Fig. S5).

Notably, γ H2AX was more active in inclusion body-negative striatal neurons in R6/2 mice at 4 wk (Fig. 9 A, bottom; and Fig. S4 C), whereas the activation extended to inclusion body-positive striatal neurons at 12 wk (Fig. 9 B and Fig. S4 C). The negative relationship between γ H2AX and inclusion bodies at 4 wk was consistent with the suppression of DNA-PK activity by soluble mutant Htt (Fig. 4 A) and with the view that inclusion bodies may be protective against HD pathology (Arrasate et al., 2004).

Furthermore, we tested DNA-PK activity and DNA-Ku70 interaction in brain tissues of nontransgenic, R6/2, and Ku70-R6/2 double-transgenic mice. DNA-PK activity and Ku70-DNA binding impaired in R6/2 mice were recovered in double-transgenic mice (Fig. 5, D and E), supporting the idea that the impairment of Ku70-mediated DNA repair contributes to the toxic effect of mutant Htt in vivo.

Discussion

In this study, beyond previously published observations on DNA damage signals (Giuliano et al., 2003; Qi et al., 2007),

mean values of four mice were compared among groups. The signals of γ H2AX in the nucleoplasm were reduced in comparison with R6/2. The γ H2AX signals were focused to the nucleoli in double-transgenic mice. *, $P < 0.01$ by Student's *t* test ($n = 4$). Error bars indicate SEM.

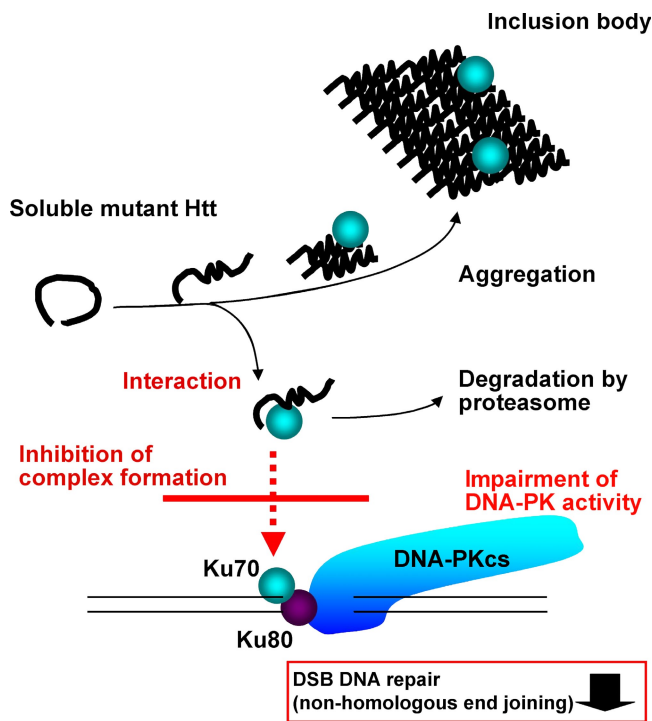


Figure 10. **A model of DNA damage repair dysfunction in the HD pathology mediated by Ku70.** Interaction between mutant Htt and Ku70 inhibits complex formation among Ku70, Ku80, and DNA-PKcs and represses the DSB repair activity of the DNA-PK complex. Ku70 bound to mutant Htt undergoes protein degradation by the proteasome system. Coaggregation to inclusion bodies also occurs, but functional impairment of the DNA-PK complex occurs more promptly by interaction before quantitative alteration of Ku70.

we found that expression of mutant Htt eventually leads to DSBs of genomic DNA in affected neurons (Fig. 1) and suggest that impairment of Ku70 contributes to the increase of DSBs in the HD pathology (Figs. 2–9). In DNA damage repair, Ku70 and Ku80 first detect DSBs and assemble at the foci. The Ku70–Ku80 heterodimer recruits DNA-PKcs and initiates the DNA damage repair reactions of XRCC4/DNAIlgase IV (Lombard et al., 2005). Mutant Htt interacts (Fig. 3, A and B) and colocalizes with Ku70 in striatal neurons in vivo (Fig. 4). In vitro assays revealed that Htt-GST but not GST protein inhibits DNA-PK activity (Fig. 5 A). Ku70 binding to DNA and Ku70–Ku80 interaction is also impaired by mutant Htt (Fig. 5, B and C). Especially soluble, rather than insoluble, mutant Htt impairs DNA-PK activity through the binding to Ku70 (Fig. 5 A). Brain tissues of R6/2 transgenic mice have a lower DNA-PK activity (Fig. 5 D). Supplementation of the Ku70 significantly rescues DNA-PK (Fig. 5 D) and degenerative phenotypes in the R6/2 mouse model of HD even though the increase of Ku70 is relatively small (Fig. 8 and Fig. 9). These results collectively suggest that Ku70 is a new critical player in the DNA damage-linked pathologies of HD (Fig. 10).

In this study, we provided direct evidence of mutant Htt-induced DSBs in primary neurons (Fig. 1 E), whereas we also used H2AX phosphorylation as the DSB marker in several experiments. Because DNA-PK was reported to phosphorylate H2AX (Stiff et al., 2004), one might ask whether

the reduced DNA-PK activity (Fig. 5) could be contradictory to H2AX phosphorylation. However, other kinases, such as ataxia telangiectasia mutated (ATM), a mediator of DNA damage-induced cell death signaling (Lombard et al., 2005; for review see Sancar et al., 2004), are also known to phosphorylate H2AX (Fernandez-Capetillo et al., 2004; Lu et al., 2006), and activation of ATM has been observed in the HD pathology (Qi et al., 2007). Therefore, our hypothesis fits very well with this experimental evidence.

Previous studies indicated that mutant Htt induces oxidative stress (for review see Lin and Beal, 2006), leading to DSBs (for review see Sancar et al., 2004). Consistently, we observed the increase of 8-oxo-dG in our primary neurons expressing mutant Htt (unpublished data). In addition, we recently found that a mitochondrial protein, Omi/HtrA2, which keeps mitochondrial homeostasis, is reduced in HD pathology (Inagaki et al., 2008). These results agree with the hypothesis that oxidative stress from mitochondria is critical for an increase of DNA damage in HD pathology. However, oxidative stress may not be the sole factor to promote DSBs. Our experiments show that impairment of DNA repair through the interaction between Ku70 and mutant Htt accelerates accumulation of DSBs and causes neuronal dysfunction from an early stage of the HD pathology. The results support DNA repair to be a critical factor promoting DSBs. This is consistent with our previous result, showing that a reduction of HMGBs essential for architectural DNA alteration (Thomas and Travers, 2001) leads to genotoxic stress (Qi et al., 2007). It is also in line with previous findings that nuclear events largely initiate polyQ pathologies (Klement et al., 1998; Saudou et al., 1998; Katsuno et al., 2003).

The R6/2 mouse is the most difficult to be remedied among various mouse models of neurodegeneration (for review see Gil and Rego, 2009). One study listed showed a lifespan elongation of 40%, the others mostly showed a minor (5–15%) or no effect. Because lifespan elongation by Ku70 reaches 30% in our study (Fig. 8 E) even though the increase of Ku70 protein in the double-transgenic mice is relatively small (Fig. 8 D), Ku70-mediated DNA repair dysfunction can be considered as a critical component among various HD pathologies in vivo. If Ku70 could be up-regulated more efficiently in a milder mouse model of HD, a higher therapeutic effect might be expected. To support this idea, we found that coexpression of Ku70 substantially elongated survival of *Drosophila* expressing mutant human Htt (unpublished data).

Several aging disorders and some autosomal recessive neurodegenerative diseases are caused by mutations of DNA repair genes. Aging disorders such as Cockayne syndrome type A (Henning et al., 1995), type B (Troelstra et al., 1992), and Werner syndrome (Oshima et al., 1996; Yu et al., 1996) are caused by mutations in DNA repair genes. The autosomal recessive cerebellar ataxias, including AOA1/EAOH (Date et al., 2001), AOA2 (Suraweera et al., 2007), and SCAN1 (Takashima et al., 2002; El-Khamisy et al., 2005), are also caused by mutations of DNA repair genes. HD seems to share DNA repair dysfunction as a critical pathology with these disorders. The difference of the HD pathology from aging disorders (de Boer et al., 2002) is that the DNA repair dysfunction is not directly or

genetically determined but indirectly or secondarily acquired by accumulation of the toxic species of mutant Htt protein.

Although some pathologies, including transcription, splicing, proteasome dysfunction, and autophagy are implicated in multiple polyQ diseases, the spectra of binding partners are clearly different among mutant polyQ proteins (Goehler et al., 2004; Lim et al., 2006). In the case of mutant Atx1, normal binding partners, including Capicua and RBM17, play critical roles in the pathology through gain of function or loss of function (Emamian et al., 2003; Lam et al., 2006; Lim et al., 2008). In our current analyses with cellular and *Drosophila* SCA1 models, the rescue effects of Ku70 on the SCA1 pathology were smaller than that on the HD pathology (unpublished data). Therefore, Ku70 seems to be a specific pathological regulator to HD at this moment. Meanwhile, DNA damage by itself is shared by the SCA1 pathology through high mobility group protein B proteins (Qi et al., 2007), and it is still possible that other molecules regulate DNA damage in SCA1 in addition to HMGBs.

Transcriptional repression in the HD pathology has been suggested by various research groups (Okazawa, 2003; Sugars and Rubinshtein, 2003; Hoshino et al., 2006). Accumulation of DNA damage causes transcriptional repression during transcription-coupled repair and induces apoptotic signals (for review see Sancar et al., 2004). Nonrepaired DSB foci will attract ATM and associated molecules (Bekker-Jensen et al., 2006), activate Chk1 and 2, and initiate apoptotic signaling (for review see Sancar et al., 2004). Insufficient function of Ku70 might also enhance ATM-mediated signaling, as persistent phosphorylation of p53 at Ser18 by the ATM activity was observed in irradiated Ku70-deficient cells in contrast to transient activation of p53 in control cells (Tomimatsu et al., 2007).

Moreover, Ku70 is known to be involved in telomere homeostasis (Laroche et al., 1998; Riha et al., 2002). It is usually localized at telomere DNA (Bailey et al., 1999; Hsu et al., 1999), whereas it relocalizes to DNA damage foci (Martin et al., 1999). The two functions seem to be controlled by distinct faces of the Ku70 molecule (Ribes-Zamora et al., 2007). Mutant Htt might disorganize the dynamism of Ku70 between telomere and DSB foci. As telomere instability is implicated in neurodegeneration (Zhang et al., 2007), the second function of Ku70 could be involved in the HD pathology. The additional functions of Ku70 other than DNA repair will be the subject of future studies.

Materials and methods

Primary neuron culture and adenovirus infection

Primary neuron culture and adenovirus constructs were performed as previously described (Qi et al., 2007). Exon 1 from the human Htt gene containing 90 or 20 CAG repeats was cleaved from pTL1HA3-CAG90 or pTL1HA3-CAG20 (Sittler et al., 2001) and subcloned into the pAxCawt cosmid (Takara Bio Inc.). During subcloning, polyQ length was further expanded to 111Q in the mutant Htt adenovirus vector. We designated the adenovirus vectors AxCA, AxCA_{111Q}, and AxCA_{20Q}. The resultant cosmids were used for the generation of adenovirus vectors by the Adenovirus Expression Vector kit (Takara Bio Inc.). After two or three amplifications, clonality of the vectors (5×10^8 – 10^9 PFU/ml) was checked by restriction enzymes and PCR. The vectors were used for infection of neurons at a multiplicity of infection of 100.

Primary neurons were prepared from the cerebral cortex of 18-d-old Wistar rat embryos (Japan SLC, Inc.). The rats were put under deep

anesthesia with ether. Their brains were dissected, minced into fine pieces, and rinsed with PBS. After incubation with 0.0125% trypsin at 37°C for 10 min, the pieces were washed twice with DME (Nissui) containing 10% fetal bovine serum, 25 mM D-glucose, 4 mM L-glutamine, and 25 µg/ml gentamycin and gently triturated with blue tips and filtered through a nylon mesh (Falcon 2350; BD) to remove any debris. Cells were seeded onto dishes (Corning) coated with poly-L-lysine (Sigma-Aldrich) at 1.8×10^5 cells/cm² and cultured at 37°C and 5% CO₂. To remove proliferating glial cells, arabinosylcytosine (Sigma-Aldrich) was added to the culture medium (4 µM) on the next day. 4 d after plating, neurons were infected by adenovirus vectors. Antioxidants, N-acetylcysteine (Sigma-Aldrich), L-γ-glutamyl-L-cysteinyl ethyl glycinate (Sigma-Aldrich), and coenzymeQ₁₀ (Sigma-Aldrich) were added 3 h after infection. The proteasome inhibitor MG-132 (Sigma-Aldrich) was dissolved in DMSO and added to the media to the appropriate final concentration of 0.3 µM. DMSO was added to the media without MG-132 as control.

Immunoblotting

For Western blot sampling, brain tissues of mutant Htt transgenic R6/2 mice [B6CBA-Tg [HD exon 1] 62Gpb/1J; The Jackson Laboratory] striatum or of nontransgenic littermate (wild type) were washed three times by ice-cold PBS and dissolved in lysis buffer containing 62.5 mM Tris/HCl, pH 6.8, 2% (wt/vol) SDS, 2.5% (vol/vol) 2-mercaptoethanol, and 5% (vol/vol) glycerol. The samples from culture cells were prepared similarly. Protein concentration was quantified by using the BCA method (Micro BCA Protein Assay Reagent kit; Thermo Fisher Scientific).

The dilution conditions of primary and secondary antibodies for immunoblotting were as follows: rabbit anti-CAG53b (1:1,000; Scherzinger et al., 1997), mouse anti-GFP (1:2,000; Takara Bio Inc.), rabbit anti-GST (1:500; Z-5; Santa Cruz Biotechnology, Inc.), mouse anti-polyQ (1:2,000; 1C2; Millipore), mouse anti-Ku70 (1:500; N3H10; Kamiya Biomedical), rabbit anti-Ku70 (1:1,000; H-308; Santa Cruz Biotechnology, Inc.), rabbit anti-Ku80 (1:1,000; H-300; Santa Cruz Biotechnology, Inc.), rabbit anti-DNA-PKcs (1:500; H-163; Santa Cruz Biotechnology, Inc.), mouse anti-γH2AX (1:500; Ser139; Millipore), rabbit anti-HD1 (1:2,000; Scherzinger et al., 1997), rabbit anti-HDAC3 (1:500; Millipore), mouse anti-GAPDH (1:10,000; Millipore), HRP-conjugated anti-goat IgG (Dako), anti-mouse IgG (GE Healthcare), and anti-rabbit IgG (1:3,000; GE Healthcare). Antibodies were diluted in TBS with Tween 20 (TBST) with 5% skim milk.

IP

For IP, cells were lysed in TNE buffer (10 mM Tris-HCl, pH 7.8, 10% NP-40, 0.15 M NaCl, and 1 mM EDTA) containing protease inhibitors (protease inhibitor cocktail; Roche) and 1 mM PMSF at 4°C for 1 h and centrifuged at 15,000 g for 20 min. The cell lysate was preincubated with protein G-Sepharose (GE Healthcare) for 2 h at 4°C and centrifuged at 15,000 g for 20 min. The supernatant lysate (1–2 µg/µl lysate protein) was incubated overnight with an appropriate antibody at 4°C and incubated with protein G-Sepharose for 2 h at 4°C. After extensive washing in TNE buffer, the Sepharose beads were collected by centrifugation at 15,000 g for 5 min and boiled in 20 µl of lysis buffer containing 0.01% bromophenol blue, and 5 µl of the eluted proteins was resolved by SDS-PAGE.

The dilution conditions of antibodies used for IP were as follows: rabbit anti-GFP (1:200; Takara Bio Inc.), rabbit anti-Ku70 (1:50; H-308; Santa Cruz Biotechnology, Inc.), 10 µg/sample rabbit antiacetylated lysine (Stressgen), mouse anti-polyQ (1:500; 1C2; Millipore), and 2 µg/sample control IgG (mouse IgG1 and rabbit IgG; Santa Cruz Biotechnology, Inc.).

Deletion constructs of Ku70

Different regions of Ku70 cDNA described in Fig. 3 C were PCR amplified and subcloned into an EcoRI-BamHI site of p3xFlag-CMV10 (Sigma-Aldrich). HEK293FT cells (Invitrogen) transfected with the Flag-Ku70 plasmid and GFP-HttQ88 plasmid were lysed with WCE buffer (50 mM Tris-HCl, pH 8.0, 280 mM NaCl, 1% NP-40, 0.2 mM EGTA, 2 mM EDTA, and 10% glycerol) 48 h after transfection. The clarified cell lysate was incubated with M2 agarose beads (Sigma-Aldrich) to purify Flag proteins by immunoaffinity. Copurified proteins were analyzed by immunoblot analysis.

Tet-on stable cell lines and quantification of induced Htt genes

To prepare tetracyclin-controlled expression plasmids, the coding region of EGFP, EGFP-HttQ17, or EGFP-HttQ88 was PCR amplified with a forward primer with BamHI site and a reverse primer with EcoRI site using pEGFP-C1 (Takara Bio Inc.), pEGFP-HttQ17, or pEGFP-HttQ88 as a template, respectively. The PCR products were subcloned into a BamHI-EcoRI site of pcDNA4/TO/Myc-His (Invitrogen). TRex-HeLa cells (Invitrogen)

were transfected with the tetracyclin-controlled expression plasmid; positive clones were selected with 200 μ g/ml zeocin in minimum essential media supplemented with 10% fetal bovine serum to establish inducible stable cell lines. Semiquantification of induced EGFP-Htt and endogenous Htt in the Tet-on stable cells was performed with 5'-GACCCTGGAAAAGCTGATGA-3' for Htt-RT-F2 and 5'-GGCTGAGGAAGCTGAGGAG-3' for Htt-RT-R1 using PfuUltra II fusion HS DNA polymerase. The following primers were used for GAPDH: GAPDH-F, 5'-GAGCCATCGCTCAGAC-3'; and GAPDH-R, 5'-GGCCATCACGCCACAGTT-3'. The PCR cycle is as follows: 95°C for 2 min, 35 cycles of 95°C for 20 s, 56°C for 20 s, 72°C for 15 s, and a final extension at 72°C for 3 min.

Preparation of nuclear and cytoplasmic proteins

To prepare the cytoplasmic and nuclear protein extracts, cultured neurons were washed three times with ice-cold PBS, pH 7.4, and centrifuged at 1,000 g for 5 min at 4°C. The cell pellets were resuspended in 8 vol of the hypotonic buffer (20 mM Hepes, pH 7.9, 10 mM KCl, 2 mM MgCl₂, 0.3% Nonidet P-40, 1 mM DTT, 1 mM EDTA, protease inhibitor cocktail [Roche], and 1 mM PMSF) and placed on ice for 20 min. The extracts were centrifuged at 15,000 g for 20 min at 4°C. The supernatants were collected as the cytoplasmic extracts. The pellets were resuspended in 50 μ l of the extraction buffer (20 mM Hepes, pH 7.9, 420 mM NaCl, 1 mM EDTA, 2 mM MgCl₂, 10% glycerol, 1 mM DTT, and protease inhibitor cocktail) and placed on ice for 20 min. The extracts were centrifuged at 15,000 g for 20 min at 4°C, and the supernatants were used as the nuclear extracts. These samples were separated by SDS-PAGE, transferred onto polyvinylidene difluoride membrane Fine Traps (Nihon Eido) by a semidry method, blocked by 5% milk in TBST (10 mM Tris/Cl, pH 8.0, 150 mM NaCl, and 0.05% Tween 20), and incubated with appropriate antibodies (see following paragraph). The filters were incubated with each primary antibody overnight at 4°C with the corresponding HRP-conjugated second antibody for 1 h at room temperature in 5% milk/TBST. Finally, the target molecules were visualized through an enhanced chemiluminescence Western blotting detection system (GE Healthcare).

Immunocytochemistry of primary neurons

Cultured neurons were fixed with 4% paraformaldehyde in 0.1 M phosphate buffer, pH 7.4, for 30 min, washed three times with PBS, blocked with 0.5% skim milk in PBS for 30 min at room temperature, and incubated with primary antibodies in PBS containing 0.5% skim milk and 0.1% Triton X-100 overnight at 4°C. The dilution conditions of primary antibodies for immunostaining were as follows: goat anti-Htt antibody (1:100; EM-48; Millipore), mouse anti- γ H2AX (1:500; Ser139; Millipore), and anti-Ku70 antibody (1:200; H-308; Santa Cruz Biotechnology, Inc.). Incubation with the secondary antibodies of Alexa Fluor 488- or 594-labeled anti-IgGs (Invitrogen) diluted at 1:500 in 0.5% skim milk in PBS was performed for 1 h at room temperature. For 8-oxo-dG (8-oxo-deoxyguanosine) staining, cells were fixed with 4% paraformaldehyde, treated with 3 M HCl for 30 min at room temperature, and washed three times with PBS. Cells were incubated with 5 mg/ml RNaseA for 1 h at room temperature, washed three times with PBS, and further incubated with anti-8-oxo-dG antibody (MOG-020P; JALCA) diluted at 1:100 in buffer G (0.3% Triton X-100 and 5% goat serum in PBS) overnight at 4°C. 8-oxo-dG signal was detected by using Alexa Fluor 594 IgG diluted at 1:1,000 in buffer G. Finally, cells were counterstained with DAPI (0.2 μ g/ml in PBS) for nuclear staining and mounted for microscopic observations (IX70; Olympus).

Immunohistochemistry of brain tissues

Brain tissues were prepared from R6/2 and mutant Htt^{99Q} knock-in mice (Htt^{97CAG + 2CGG}) whose phenotype onset is \sim 45 wk (Ishiguro et al., 2001; Sawada et al., 2007). Mouse brains were fixed in 4% paraformaldehyde for 12–16 h. For human pathology, HD human patient brains and nonneurological disease brains (leukemia or pneumonia) were used for analysis with agreement of their family and approval of the ethics committee. The paraffin-embedded mouse sections were deparaffinized, rehydrated, and microwaved in 10 mM of citrate buffer, pH 6.0, at 120°C for 15 min. These sections were incubated sequentially with 3% hydrogen peroxide for 20 min at room temperature to inhibit endogenous peroxidase followed by incubation with primary antibodies overnight at 4°C and finally with Alexa Fluor 488- and 594-labeled anti-IgGs (Invitrogen) for 1 h at room temperature. Signal intensity per cell was calculated as described in the following section. More than 100 cells from at least three different slides were measured. To exclude background fluorescence, we measured fluorescence of 10 randomly selected noncell-existing tissue areas of each sample, and their mean value was subtracted from the fluorescence of cells on the same slide. The dilution conditions of primary antibodies

for immunostaining were as follows: mouse anti- γ H2AX antibody (1:500; Ser139; Millipore), rabbit anti-Ku70 antibody (1:200; H-308; Santa Cruz Biotechnology, Inc.), mouse anti-Htt antibody (1:100; EM-48; Millipore), rabbit anti-Htt antibody CAG53b (1:400), biotin-conjugated mouse anti-NeuN antibody (1:100; Millipore), and rabbit antifibrillar (1:200; Abcam).

Quantification of immunostain signals

The digital images were collected using a living cell imaging system of microscopy (IX71; Olympus) with a UPlan S Apo 20 \times 0.75 NA and 40 \times 0.90 NA objective lens and a charge-coupled device camera (DP30BW; Olympus) at room temperature. The fluorescence signal intensities of immunostained neurons (NeuN-positive cells) were calculated from at least three different slides of a brain sample, and >100 cells were measured in each sample by MetaMorph software (Universal Imaging Corporation). The signal intensity per cell was calculated by demarcating the cell nucleus. Mean pixel intensities within the image were measured, and background signals were subtracted. To calculate background signals, we measured fluorescence of 10 randomly selected noncell-existing tissue areas of each slide, and their mean value was subtracted from the cellular fluorescence signals on the same slide. The mean of the signal intensities after background subtraction was calculated in each brain sample, and the mean values of each group (mouse brain samples, $n = 4-6$; human brain samples, $n = 3$) were statistically analyzed between the groups. Acquired images were processed with Photoshop software (Adobe).

Confocal images were acquired at room temperature using a confocal laser-scanning microscope (LSM 510 Meta; Carl Zeiss, Inc.) and a 63 \times 1.4 NA oil immersion objective lens and processed using LSM image browser (Carl Zeiss, Inc.). Signal intensity profiles for Fig. 4 C were also obtained using LSM image browser, and the background signal intensity was subtracted from the signals. Brightness, contrast, and γ of the acquired images were adjusted with LSM image browser and Photoshop software.

Comet assay

DNA DSBs were evaluated using the neutral single-cell gel electrophoresis assay (comet assay) as described previously (Olive and Banáth, 2006) with minor modifications (CometAssay; Trevigen). Cells were harvested, suspended with ice-cold PBS at 5×10^5 /ml, mixed with 1% low melting point agarose at a ratio of 1:10 (vol/vol), and spread gently onto a coverslip to avoid creating bubbles. The agarose was allowed to solidify at 4°C, and the slides were immersed in ice-cold fresh lysis solution for 30 min at 4°C in a dark chamber. After lysis, the slides were equilibrated for 20 min with TBE buffer (90 mM Tris, 90 mM boric acid, and 2 mM EDTA, pH 8.0), and electrophoresis was performed in TBE buffer at 27 V for 20 min. After electrophoresis, the slides were air dried at room temperature; then, individual cells were stained with SYBR green I solution and viewed using a UV light fluorescence microscope. Quantification was achieved by analyzing at least 50 randomly selected comets per slide with the Comet software (National Institutes of Health) using the following parameters: tail length (estimated leading edge from the nucleus in micrometers), L/H (the ratio of tail length to head diameter), and tail moment (arbitrary units; defined as the product of the percentage of DNA in the tail multiplied by the tail length).

We used CPT as a positive control in the neutral comet assay because CPT initially forms nicks in genome DNA through inhibition of Top1. Top1 relieves torsion stress of DNA by nick formation with the cleavage complex (Wang, 2002). Although Top1 cleavage complexes are normally very short lived and the nick is normally repaired by TDP1 and other factors, the nick leads to Top1-linked SSBs or DSBs by collision of the Top1 cleavage complex with the transcription or replication machinery. CPT treatment increases the half-life of the Top1 cleavage complex and similarly induces Top1-associated SSBs and DSBs (Katyal et al., 2007). Furthermore, a recent study showed that CPT induces DSBs in postmitotic primary neurons (Sordet et al., 2009). All of these previous results support the usage of CPT as a positive control.

Coprecipitation assay

Transfection into HeLa and HEK293 cells was performed with Lipofectamine 2000 (Invitrogen) according to the manufacturer's instructions and cultured for another 2 d. For Fig. S1 C, HEK293 cells were cultured in DME supplemented with 10% fetal bovine serum at 37°C and 5% CO₂. pFlag-CMV-D11-Htt (N-terminal 506 amino acids containing 145 glutamines) and pcMyc-CMV-D12-Ku70 were cotransfected using Lipofectamine 2000 (Invitrogen) following the manufacturer's instructions. After 48 h of transfection, the cells were pelleted and lysed in IP buffer (50 mM Tris, pH 7.6, 150 mM NaCl, 1% Triton X-100, and 10% glycerol) in the presence of protease inhibitor cocktail (Roche). Mouse IgG-coated magnetic beads (Dynabeads M-280; Invitrogen) were washed three times using IP buffer.

750 µg cell lysate was incubated with 2 µl specific antibody (monoclonal anti-Flag [Sigma-Aldrich] and 9E10 c-Myc) for 1 h at 4°C. Antibody-bound protein complexes were isolated by incubating with 40 µl of the beads for 1 h at 4°C. Subsequently, the beads were separated from the lysate and washed one time using IP buffer. The protein complexes were heat denatured and analyzed by SDS-PAGE and Western blotting.

Ku70-shRNA knockdown and EGFP-Htt expression vectors

An artificial oligo DNA (5'-GAATTCGGAAGAGATAGTTGATTGTGTCGTCCAAATCAAATCTCTTCCTTTTTGGATCC-3') was designed from the sequence of siRNA against human Ku70 (Applied Biosystems) by addition of a loop and termination signal sequences. The complementary oligo was also synthesized, and the double strand subcloned between EcoRI-BamHI sites of pSIREN-DsRed-Express (BD).

The cDNA fragments encoding exon 1 of human Htt gene with 17 or 88 CAG repeats were amplified by PCR as previously described (Sittler et al., 2001) and subcloned into pEGFP-C1 plasmid (Takara Bio Inc.). After verification by sequencing, the plasmids were transfected into HeLa cells maintained in DME supplemented with 10% fetal bovine serum. Transfection was performed with Lipofectamine 2000 (Invitrogen) according to the manufacturer's instructions and cultured for another 2 d. The protein expression level was confirmed by immunoblotting cell lysates with antibodies against tagged EGFP proteins.

LUMIER assay

All of the cDNAs used in the LUMIER assay were subcloned into the LUMIER plasmids pPAREni-DM and pFireV5-DM using GATEWAY technology. Human embryonic kidney HEK293 cells were seeded in 96-well plates and cultured in DME supplemented with 10% fetal bovine serum at 37°C and 5% CO₂. Cotransfection of the plasmids was performed using Lipofectamine 2000 (Invitrogen) following the manufacturer's protocol. The analyses described in the following paragraph were performed after 24 h of transfection.

For the LUMIER assay, cells were lysed at 4°C for 40 min in 100 µl of lysis buffer containing 50 mM Hepes-KOH, pH 7.4, 150 mM NaCl, 0.1% NP-40, 1.5 mM MgCl₂, 1 mM EDTA, 1 mM DTT, and 75 U/ml benzonase (Merck) in the presence of protease inhibitor cocktail (Roche). Cell extracts were prepared and assessed for the expression of the fusion proteins by luciferase assays. Protein complexes were isolated from 80 µl cell extracts using 5 µl IgG-coated magnetic beads (M-280 sheep anti-rabbit IgG; Dynabeads; Invitrogen) and subsequently washed with 100 µl PBS. Binding (co-IP) of the firefly-V5-tagged fusion proteins to the PA-Renilla-tagged Ku70 was quantified by measuring the firefly luciferase activity in a luminescence plate reader (TECAN Infinite M200) using the Dual-Glo Luciferase Assay system (Promega). Renilla luciferase activity was also measured as a control for PA-Renilla luciferase binding to the IgG-coated magnetic beads. Each experiment was performed as triplicate transfection.

GST fusion proteins

Wild-type or mutant exon 1 cDNA (nucleotides 341–511) of the human HD gene (The Huntington's Disease Collaborative Research Group, 1993) was amplified from the cosmid vectors by PCR using primers (forward) 5'-AAAGGATCCAGGCTTCGAGTCCCTC-3' and (reverse) 5'-AAAGAATTCGCCGGCCGGGTGGCGG-3' and subcloned into the BamHI-EcoRI sites of the expression vector pGEX-3X (GE Healthcare). The plasmids were verified by sequencing to have either 20 or 110 CAG repeats. During PCR, the number of CAG repeats was changed from 111 to 110 in mutant cDNA.

Escherichia coli cells (BL21) were transformed with the plasmid, grown to an OD₆₀₀ of 0.6, and the fusion protein was induced with 0.5 mM IPTG for 3.5 h according to the manufacturer's protocol (GE Healthcare). GST fusion proteins were purified by BugBuster GST Bind Purification kit (EMD). 400 ml cultures of induced bacteria were centrifuged at 5,000 g for 30 min at 4°C, and the resulting pellets were resuspended in BugBuster reagent (5 ml reagent/g wet cell paste) containing 0.1 mg/ml lysozyme, 25 U/ml benzonase nuclease, and protease inhibitors (protease inhibitor cocktail; Roche). After 20 min at room temperature, cells were centrifuged at 16,000 g for 30 min at 4°C. The supernatant was incubated with 2 ml 50% slurry of GST bind resin that had been washed three times with GST bind/wash buffer for 1 h and poured into a small column and washed with 10 ml GST bind/wash buffer. The bound fusion protein was eluted with 2 ml of GST elution buffer and stored at -80°C until use. The original pellet was suspended with the same volume of BugBuster reagent containing 0.1 mg/ml lysozyme and incubated for 10 min at room temperature. 6 vol diluted BugBuster

reagent (diluted 1:10 in deionized water) was added. The suspension was vortexed for 1 min and centrifuged at 5,000 g for 15 min at 4°C. The pellet was suspended with diluted BugBuster reagent and centrifuged at 16,000 g for 20 min at 4°C. This wash step was repeated three times, and the final pellet was stored at -80°C until use. Protein concentration was quantified by using the BCA method, and expression levels of encoded proteins were examined by immunoblotting.

DNA-dependent protein kinase activity assay

Nuclear extract was isolated from HeLa cells with a Nuclear Extraction kit (Active Motif) or from mouse cerebral cortex and striatum by the previously described method of Dignam et al. (1983). DNA-PK activity was determined by a DNA-PK assay system (SignaTECT; Promega) according to the manufacturer's instructions with minor modifications. In brief, 0.4 mM biotinylated peptide substrate in a reaction buffer containing 50 mM Hepes, pH 7.5, 100 mM KCl, 10 mM MgCl₂, 0.1 mM EDTA, 0.2 mM EGTA, 1 mM DTT, 0.1 mM ATP, and 0.5 µCi γ-[³²P]ATP was added to a DNA-PK activation buffer (0.25 µg calf thymus) or a control buffer (1 mM Tris-HCl, pH 7.4, and 0.1 mM EDTA, pH 8.0) and preincubated at 30°C for 5 min. Reactions were initiated by adding the preincubated mixture to 10 µl DNA-PK solution containing 116 U DNA-PK (purified from HeLa cells; Promega) and appropriate amounts of GST, GST-Htt20Q, and GST-Htt110Q. The final volume was adjusted to 25 µl and incubated at 30°C for 20 min. Reactions were stopped with 12.5 µl of termination buffer (2.5 M guanidine hydrochloride) and spotted onto biotin capture membranes (SAM2; Promega). Membranes were washed in 2 M NaCl, in 2 M NaCl in 1% H₃PO₄, and finally in deionized water. Radioactivity was analyzed using a phosphorimaging system (Bass FL3000; Fujifilm) as the counts of ³²P incorporated in the presence of DNA minus the counts of ³²P incorporated in the absence of DNA. The DNA-PK activity was calculated as described in the kit protocol.

As the substrate peptide is known to be a target for the PI3-kinase family members ATM, ATM related, and DNA-PK (Lees-Miller et al., 1992; Canman et al., 1998; Tibbetts et al., 1999), to demonstrate the specificity of DNA activation of the enzyme activity, the extracts (75 µg protein) were preincubated with active or inactive (heat inactivated at 80°C for 30 min) 0.1% DNase I (Roche) for 2 h at 4°C. The DNA-PK enzymatic activity was determined by subtracting the activity in the extract incubated with active DNase I from that incubated with inactive one.

Ku70-DNA-binding activity

The Ku70-DNA-binding activity was analyzed by Ku70-Ku86 DNA repair kit (Active Motif) according to the manufacturer's instructions. Nuclear extract was isolated from HeLa cells with a nuclear extraction kit (Active Motif) or from mouse cerebral cortex and striatum by the previously described method of Dignam et al. (1983). The HeLa nuclear extract (5 µg protein) and 150 ng GST, GST-Htt20Q, or GST-Htt110Q protein were mixed and incubated for 60 min at room temperature in the oligonucleotide-coated 96-well plate. After three steps of washing, Ku70 antibody was added followed by the HRP-conjugated secondary antibody. Each antibody was incubated for 60 min at room temperature. After four steps of washing, developing and stop solutions were added. Optical density was measured by spectrophotometer at 450 nm. The data represent the mean ± SD of three separate determinations. For the detection of Ku70-DNA-binding activity in mouse brain, 75 µg nuclear extract prepared from cerebral cortex and striatum was directly loaded into the plate. The Ku70-DNA-binding activity was detected as described in the previous paragraph.

Ku70-Ku80 interaction

IP and immunoblotting methods are described in the previous paragraph.

Inducible expression of mutant Htt

The pTRE-Tight-BI-DsRed-Htt103Q plasmid was generated by subcloning human HD exon 1 cDNA digested from pTL1HA3-HD90Q (Sittler et al., 2001) into pTRE-Tight-BI-DsRed vector (Takara Bio Inc.). During the subcloning, CAG repeats were expanded to 103. GFP-H2AX was described previously (Siino et al., 2002). pTet-on (Takara Bio Inc.) and pTRE-Tight-BI-DsRed-Htt103Q were cotransfected to HeLa cells. Expression of Htt and DsRed was induced by 1 µg/ml doxycycline.

Cdk1 and MAPK assay

The cells were washed three times with PBS and lysed by cell lysis buffer composed of 50 mM Tris HCl, pH 7.5, 150 mM NaCl, 1 mM EDTA, 1 mM EGTA, 1% Triton X-100, 2.5 mM sodium pyrophosphate, 10 mM β-glycerophosphate, 1 mM Na₃VO₄, protease inhibitor cocktail (Roche),

and 1 mM PMSF at 4°C. The cell lysate was stored at -80°C until use. For Cdk1 kinase assay, 500 µl of protein samples (containing 650 µg protein) was incubated with 20 µl HCK gel (MBL International) for 2 h at 4°C. The gel was washed three times with cell lysis buffer and twice with wash buffer (25 mM Hepes, pH 7.5, and 10 mM MgCl). The gel was mixed with kinase assay buffer composed of 25 mM Hepes, pH 7.5, 10 mM MgCl, 10% (vol/vol) mouse vimentin peptide solution (SLYSSPGGAYC; MBL International), and 0.1 mM ATP (Sigma-Aldrich), and the mixture was incubated for 30 min at 30°C. The reaction was terminated by the addition of 200 µl PBS containing 50 mM EGTA. The phosphorylation of mouse vimentin peptides was detected using an ELISA MESACUP Cdc2/Cdk1 kinase assay kit (MBL International) according to the manufacturer's protocol. For MAPK assay, 500 µl of protein samples (containing 500 µg protein) was incubated with 10 µl anti-MAPK/Erk1/2 agarose and conjugated (Millipore) for 2 h at 4°C. The gel was washed three times with cell lysis buffer and twice with wash buffer composed of 20 mM MOPS, pH 7.2, 25 mM β-glycerophosphate, 5 mM EGTA, 1 mM Na₃VO₄, and 1 mM DTT. The kinase assay was performed using a MAPK/Erk IP kinase assay kit (Millipore) according to the manufacturer's protocol.

Generation of transgenic mice

To generate transgenic mice overexpressing mouse Ku70 in the nervous system, the RIKEN mouse FANTOM clone encoding full-length mouse Ku70 was inserted downstream of the enhancer/promoter of the rat NSE gene (promoter; nucleotides 146,320,892–146,318,938 of AC_000072). The 1.9-kb sequence upstream of the rat NSE gene, which had been identified as the NSE enhancer/promoter (Forss-Petter et al., 1990), was subcloned from the genome DNA of Brown Norway and Sprague-Dawley rats and inserted into pRES-hrGFPII (Agilent Technologies) by replacing the cytomegalovirus promoter with Spel and EcoRI sites. The full-length mouse Ku70 cDNA was inserted downstream of the NSE enhancer/promoter in pRES-hrGFPII, which also includes the internal ribosome entry site and humanized recombinant GFPII. To distinguish endogenous and transgenic Ku70, a 3xFlag tag sequence was added to the C terminus of Ku70 cDNA. The plasmid was digested with AclI and SgrAI, and the resultant 5.5-kb fragment was injected into fertilized mouse oocytes derived from C57BL/6 mice.

Ku70 transgenic mice (C57BL/6) were crossed with CBA mice to generate Ku70 transgenic male mice in the CBA × C57BL/6 background. Double-transgenic mice of Ku70 and mutant Htt (CBA × C57BL/6) were generated by crossing Ku70 transgenic male mice (CBA × C57BL/6) and R6/2 ovarian-transplanted female mice (CBA × C57BL/6). The R6/2 mouse line was maintained by crossing R6/2 ovarian-transplanted female with CBA × C57BL/6 male mice.

Genomic DNA was extracted from the tail, and R6/2 mice were identified by PCR as described previously (Mangiarini et al., 1996). For genotyping of Ku70 transgenic mice, PCR was performed with the primers (forward) 5'-CCTCGAGGAATTCAGCAAAC-3' and (reverse) 5'-GATTCGAACATAGCCCTGGA-3' that amplify the 200-bp sequence from the NSE promoter to the Ku70 gene. Amplification was performed with Ex-Taq (Takara Bio Inc.); the condition was 94°C for 30 s for denaturing, 58°C for 1 min for annealing, and 72°C for 30 s for extension by 45 cycles. The size of the product was ~200 bp. The protein expression from the transgene was confirmed by Western blotting by using antibodies against anti-Flag (1:3,000; F3165; Sigma-Aldrich) and anti-Ku70 (1:500; H308; Santa Cruz Biotechnology, Inc.).

Mouse behavioral tests

For the rotarod test, mice were placed on a rotating rod (3.5 rpm), and the rotating speed was linearly increased to 35 rpm at 300 s and continued at 35 rpm until 360 s (for 4- to 12-wk-old mice). Mice received three trials per day for three consecutive days. The mean latency to fall off the rotarod was recorded and used for subsequent analyses. For the footprint test, steps of the hind paws were recorded with ink during walking. The resulting footprint tracings were analyzed, measuring stride length for hind paws. Each measurement represented the mean over three steps. For the clasping test, mice were observed in 2-s time bins for 14 s. Each mouse was allocated a score of 1 for abnormal hindlimb movement and score of 0 in the absence of any abnormal movement. This allowed for a maximum score of 7. Behavioral data were subjected to one-way analysis of variance with genotype as the factor at each time point followed by a Bonferroni post hoc test. Survival curves were analyzed by the Kaplan-Meier method using Statcel2 software; the survival ratio was statistically compared by log-rank test.

Online supplemental material

Fig. S1 shows activation of H2AX and 53BP1 in the nuclei of striatal neurons of R6/2 mice. Fig. S2 shows interaction between Ku70 and

full-length mutant Htt protein. Fig. S3 shows suppression of DNA-PK activity by GST-Htt111Q fusion protein. Fig. S4 shows additional data of Ku70-R6/2 double-transgenic mice. Fig. S5 shows nucleolar localization of γH2AX in striatal neurons of Ku70-R6/2 double-transgenic mice. Online supplemental material is available at <http://www.jcb.org/cgi/content/full/jcb.200905138/DC1>.

We thank Dr. Dena Johnson-Schlitz and Dr. William Engels (University of Wisconsin, Madison, WI) for gDmKu70 transgenic flies, Dr. Juan Botas (Baylor College of Medicine, Houston, TX) for Atx1 transgenic flies, and Mrs. Tayoko Tajima for her excellent technical support. We also thank Professor Frederick Alt (Howard Hughes Medical Institute, Harvard Medical School, Boston, MA) for providing Ku70 knockout mice.

This work was supported by grants to H. Okazawa from the Japan Science and Technology Agency (PRESTO; Core Research for Evolutional Science and Technology), the Ministry of Education, Culture, Sports, Science and Technology of Japan (grants 16390249, 16650076, 18390254, and 18650097 and Research on Pathomechanisms of Brain Disorders grants 17025017, 18023014, and 20023011), Tokyo Biochemical Research Foundation, Mitsubishi Parma Research Foundation, and The Uehara Memorial Foundation.

Submitted: 31 May 2009

Accepted: 6 April 2010

References

- Arrasate, M., S. Mitra, E.S. Schweitzer, M.R. Segal, and S. Finkbeiner. 2004. Inclusion body formation reduces levels of mutant huntingtin and the risk of neuronal death. *Nature*. 431:805–810. doi:10.1038/nature02998
- Bae, B.I., H. Xu, S. Igarashi, M. Fujimuro, N. Agrawal, Y. Taya, S.D. Hayward, T.H. Moran, C. Montell, C.A. Ross, et al. 2005. p53 mediates cellular dysfunction and behavioral abnormalities in Huntington's disease. *Neuron*. 47:29–41. doi:10.1016/j.neuron.2005.06.005
- Bailey, S.M., J. Meyne, D.J. Chen, A. Kurimasa, G.C. Li, B.E. Lehnert, and E.H. Goodwin. 1999. DNA double-strand break repair proteins are required to cap the ends of mammalian chromosomes. *Proc. Natl. Acad. Sci. USA*. 96:14899–14904. doi:10.1073/pnas.96.26.14899
- Barrios-Rodiles, M., K.R. Brown, B. Ozdamar, R. Bose, Z. Liu, R.S. Donovan, F. Shinjo, Y. Liu, J. Dembowy, I.W. Taylor, et al. 2005. High-throughput mapping of a dynamic signaling network in mammalian cells. *Science*. 307:1621–1625. doi:10.1126/science.1105776
- Bekker-Jensen, S., C. Lukas, R. Kitagawa, F. Melander, M.B. Kastan, J. Bartek, and J. Lukas. 2006. Spatial organization of the mammalian genome surveillance machinery in response to DNA strand breaks. *J. Cell Biol.* 173:195–206. doi:10.1083/jcb.200510130
- Bennett, E.J., T.A. Shaler, B. Woodman, K.Y. Ryu, T.S. Zaitseva, C.H. Becker, G.P. Bates, H. Schulman, and R.R. Kopito. 2007. Global changes to the ubiquitin system in Huntington's disease. *Nature*. 448:704–708. doi:10.1038/nature06022
- Bianchi, M.E., and A. Agresti. 2005. HMG proteins: dynamic players in gene regulation and differentiation. *Curr. Opin. Genet. Dev.* 15:496–506. doi:10.1016/j.gde.2005.08.007
- Browne, S.E., R.J. Ferrante, and M.F. Beal. 1999. Oxidative stress in Huntington's disease. *Brain Pathol.* 9:147–163.
- Butler, R., and G.P. Bates. 2006. Histone deacetylase inhibitors as therapeutics for polyglutamine disorders. *Nat. Rev. Neurosci.* 7:784–796. doi:10.1038/nrn1989
- Byrum, J., S. Jordan, S.T. Safrany, and W. Rodgers. 2004. Visualization of inositol phosphate-dependent mobility of Ku: depletion of the DNA-PK cofactor InsP6 inhibits Ku mobility. *Nucleic Acids Res.* 32:2776–2784. doi:10.1093/nar/gkh592
- Canman, C.E., D.S. Lim, K.A. Cimprich, Y. Taya, K. Tamai, K. Sakaguchi, E. Appella, M.B. Kastan, and J.D. Siliciano. 1998. Activation of the ATM kinase by ionizing radiation and phosphorylation of p53. *Science*. 281:1677–1679. doi:10.1126/science.281.5383.1677
- Cohen, H.Y., S. Lavu, K.J. Bitterman, B. Hekking, T.A. Imahiyero, C. Miller, R. Frye, H. Ploegh, B.M. Kessler, and D.A. Sinclair. 2004. Acetylation of the C terminus of Ku70 by CBP and PCAF controls Bax-mediated apoptosis. *Mol. Cell*. 13:627–638. doi:10.1016/S1097-2765(04)00094-2
- Cui, L., H. Jeong, F. Borovecki, C.N. Parkhurst, N. Tanese, and D. Krainc. 2006. Transcriptional repression of PGC-1α by mutant huntingtin leads to mitochondrial dysfunction and neurodegeneration. *Cell*. 127:59–69. doi:10.1016/j.cell.2006.09.015
- Dastoor, Z., and J.-L. Dreyer. 2001. Potential role of nuclear translocation of glyceraldehyde-3-phosphate dehydrogenase in apoptosis and oxidative stress. *J. Cell Sci.* 114:1643–1653.

- Date, H., O. Onodera, H. Tanaka, K. Iwabuchi, K. Uekawa, S. Igarashi, R. Koike, T. Hiroi, T. Yuasa, Y. Awaya, et al. 2001. Early-onset ataxia with ocular motor apraxia and hypoalbuminemia is caused by mutations in a new HIT superfamily gene. *Nat. Genet.* 29:184–188. doi:10.1038/ng1001-184
- de Boer, J., J.O. Andressoo, J. de Wit, J. Huijman, R.B. Beems, H. van Steeg, G. Weeda, G.T. van der Horst, W. van Leeuwen, A.P. Themmen, et al. 2002. Premature aging in mice deficient in DNA repair and transcription. *Science*. 296:1276–1279. doi:10.1126/science.1070174
- Di Prospero, N.A., and K.H. Fischbeck. 2005. Therapeutics development for triplet repeat expansion diseases. *Nat. Rev. Genet.* 6:756–765. doi:10.1038/nrg1690
- Dignam, J.D., R.M. Lebovitz, and R.G. Roeder. 1983. Accurate transcription initiation by RNA polymerase II in a soluble extract from isolated mammalian nuclei. *Nucleic Acids Res.* 11:1475–1489. doi:10.1093/nar/11.5.1475
- El-Khamisy, S.F., G.M. Saifi, M. Weinfeld, F. Johansson, T. Helleday, J.R. Lupski, and K.W. Caldecott. 2005. Defective DNA single-strand break repair in spinocerebellar ataxia with axonal neuropathy-1. *Nature*. 434:108–113. doi:10.1038/nature03314
- Emamian, E.S., M.D. Kaytor, L.A. Duvick, T. Zu, S.K. Tousey, H.Y. Zoghbi, H.B. Clark, and H.T. Orr. 2003. Serine 776 of ataxin-1 is critical for polyglutamine-induced disease in SCA1 transgenic mice. *Neuron*. 38:375–387. doi:10.1016/S0896-6273(03)00258-7
- Fairbairn, D.W., P.L. Olive, and K.L. O'Neill. 1995. The comet assay: a comprehensive review. *Mutat. Res.* 339:37–59.
- Fernandez-Capetillo, O., A. Lee, M. Nussenzweig, and A. Nussenzweig. 2004. H2AX: the histone guardian of the genome. *DNA Repair (Amst.)*. 3:959–967. doi:10.1016/j.dnarep.2004.03.024
- Forss-Petter, S., P.E. Danielson, S. Catsicas, E. Battenberg, J. Price, M. Nerenberg, and J.G. Sutcliffe. 1990. Transgenic mice expressing beta-galactosidase in mature neurons under neuron-specific enolase promoter control. *Neuron*. 5:187–197. doi:10.1016/0896-6273(90)90308-3
- Gauthier, L.R., B.C. Charrin, M. Borrell-Pagès, J.P. Dompierre, H. Rangone, F.P. Cordelières, J. De Mey, M.E. MacDonald, V. Lessmann, S. Humbert, and F. Saudou. 2004. Huntingtin controls neurotrophic support and survival of neurons by enhancing BDNF vesicular transport along microtubules. *Cell*. 118:127–138. doi:10.1016/j.cell.2004.06.018
- Gil, J.M., and A.C. Rego. 2009. The R6 lines of transgenic mice: a model for screening new therapies for Huntington's disease. *Brain Res. Brain Res. Rev.* 59:410–431. doi:10.1016/j.brainresrev.2008.12.001
- Giorgini, F., P. Guidetti, Q. Nguyen, S.C. Bennett, and P.J. Muchowski. 2005. A genomic screen in yeast implicates kynurenine 3-monooxygenase as a therapeutic target for Huntington disease. *Nat. Genet.* 37:526–531. doi:10.1038/ng1542
- Giuliano, P., T. De Cristofaro, A. Affaitati, G.M. Pizzulo, A. Feliciello, C. Criscuolo, G. De Michele, A. Filla, E.V. Avvedimento, and S. Varrone. 2003. DNA damage induced by polyglutamine-expanded proteins. *Hum. Mol. Genet.* 12:2301–2309. doi:10.1093/hmg/ddg242
- Goehler, H., M. Lalowski, U. Stelzl, S. Waelter, M. Stroedicke, U. Worm, A. Droege, K.S. Lindenberg, M. Knoblich, C. Haenig, et al. 2004. A protein interaction network links GIT1, an enhancer of huntingtin aggregation, to Huntington's disease. *Mol. Cell*. 15:853–865. doi:10.1016/j.molcel.2004.09.016
- Gu, Y., J. Sekiguchi, Y. Gao, P. Dikkes, K. Frank, D. Ferguson, P. Hasty, J. Chun, and F.W. Alt. 2000. Defective embryonic neurogenesis in Ku-deficient but not DNA-dependent protein kinase catalytic subunit-deficient mice. *Proc. Natl. Acad. Sci. USA*. 97:2668–2673. doi:10.1073/pnas.97.6.2668
- Henning, K.A., L. Li, N. Iyer, L.D. McDaniel, M.S. Reagan, R. Legerski, R.A. Schultz, M. Stefanini, A.R. Lehmann, L.V. Mayne, and E.C. Friedberg. 1995. The Cockayne syndrome group A gene encodes a WD repeat protein that interacts with CSB protein and a subunit of RNA polymerase II TFIIH. *Cell*. 82:555–564. doi:10.1016/0092-8674(95)90028-4
- Hoshino, M., M.L. Qi, N. Yoshimura, T. Miyashita, K. Tagawa, Y. Wada, Y. Enokido, S. Marubuchi, P. Harjes, N. Arai, et al. 2006. Transcriptional repression induces a slowly progressive atypical neuronal death associated with changes of YAP isoforms and p73. *J. Cell Biol.* 172:589–604. doi:10.1083/jcb.200509132
- Hsu, H.L., D. Gilley, E.H. Blackburn, and D.J. Chen. 1999. Ku is associated with the telomere in mammals. *Proc. Natl. Acad. Sci. USA*. 96:12454–12458. doi:10.1073/pnas.96.22.12454
- Illuzzi, J., S. Yerkes, H. Parekh-Olmedo, and E.B. Kmieciak. 2009. DNA breakage and induction of DNA damage response proteins precede the appearance of visible mutant huntingtin aggregates. *J. Neurosci. Res.* 87:733–747. doi:10.1002/jnr.21881
- Inagaki, R., K. Tagawa, M.L. Qi, Y. Enokido, H. Ito, T. Tamura, S. Shimizu, K. Oyanagi, N. Arai, I. Kanazawa, et al. 2008. Omi / HtrA2 is relevant to the selective vulnerability of striatal neurons in Huntington's disease. *Eur. J. Neurosci.* 28:30–40. doi:10.1111/j.1460-9568.2008.06323.x
- Ira, G., A. Pelliccioli, A. Balijja, X. Wang, S. Fiorani, W. Carotenuto, G. Liberi, D. Bressan, L. Wan, N.M. Hollingsworth, et al. 2004. DNA end resection, homologous recombination and DNA damage checkpoint activation require CDK1. *Nature*. 431:1011–1017. doi:10.1038/nature02964
- Ishiguro, H., K. Yamada, H. Sawada, K. Nishii, N. Ichino, M. Sawada, Y. Kurosawa, N. Matsushita, K. Kobayashi, J. Goto, et al. 2001. Age-dependent and tissue-specific CAG repeat instability occurs in mouse knock-in for a mutant Huntington's disease gene. *J. Neurosci. Res.* 65:289–297. doi:10.1002/jnr.1153
- Iwata, A., J.C. Christianson, M. Bucci, L.M. Ellerby, N. Nukina, L.S. Forno, and R.R. Kopito. 2005. Increased susceptibility of cytoplasmic over nuclear polyglutamine aggregates to autophagic degradation. *Proc. Natl. Acad. Sci. USA*. 102:13135–13140. doi:10.1073/pnas.0505801102
- Jackson, G.R., I. Salecker, X. Dong, X. Yao, N. Arnheim, P.W. Faber, M.E. MacDonald, and S.L. Zipursky. 1998. Polyglutamine-expanded human huntingtin transgenes induce degeneration of *Drosophila* photoreceptor neurons. *Neuron*. 21:633–642. doi:10.1016/S0896-6273(00)80573-5
- Jin, S., and D.T. Weaver. 1997. Double-strand break repair by Ku70 requires heterodimerization with Ku80 and DNA binding functions. *EMBO J.* 16:6874–6885. doi:10.1093/emboj/16.22.6874
- Johnston, J.A., C.L. Ward, and R.R. Kopito. 1998. Aggresomes: a cellular response to misfolded proteins. *J. Cell Biol.* 143:1883–1898. doi:10.1083/jcb.143.7.1883
- Ju, B.G., V.V. Lunyak, V. Perissi, I. Garcia-Bassets, D.W. Rose, C.K. Glass, and M.G. Rosenfeld. 2006. A topoisomerase II β -mediated dsDNA break required for regulated transcription. *Science*. 312:1798–1802. doi:10.1126/science.1127196
- Katsuno, M., H. Adachi, M. Doyu, M. Minamiyama, C. Sang, Y. Kobayashi, A. Inukai, and G. Sobue. 2003. Leuprorelin rescues polyglutamine-dependent phenotypes in a transgenic mouse model of spinal and bulbar muscular atrophy. *Nat. Med.* 9:768–773. doi:10.1038/nm878
- Katyal, S., S.F. el-Khamisy, H.R. Russell, Y. Li, L. Ju, K.W. Caldecott, and P.J. McKinnon. 2007. TDP1 facilitates chromosomal single-strand break repair in neurons and is neuroprotective in vivo. *EMBO J.* 26:4720–4731. doi:10.1038/sj.emboj.7601869
- Klement, I.A., P.J. Skinner, M.D. Kaytor, H. Yi, S.M. Hersch, H.B. Clark, H.Y. Zoghbi, and H.T. Orr. 1998. Ataxin-1 nuclear localization and aggregation: role in polyglutamine-induced disease in SCA1 transgenic mice. *Cell*. 95:41–53. doi:10.1016/S0092-8674(00)81781-X
- Kovtun, I.V., Y. Liu, M. Bjoras, A. Klungland, S.H. Wilson, and C.T. McMurray. 2007. OGG1 initiates age-dependent CAG trinucleotide expansion in somatic cells. *Nature*. 447:447–452. doi:10.1038/nature05778
- Lam, Y.C., A.B. Bowman, P. Jafar-Nejad, J. Lim, R. Richman, J.D. Fryer, E.D. Hyun, L.A. Duvick, H.T. Orr, J. Botas, and H.Y. Zoghbi. 2006. ATAXIN-1 interacts with the repressor Capicua in its native complex to cause SCA1 neuropathology. *Cell*. 127:1335–1347. doi:10.1016/j.cell.2006.11.038
- Laroche, T., S.G. Martin, M. Gotta, H.C. Gorham, F.E. Pryde, E.J. Louis, and S.M. Gasser. 1998. Mutation of yeast Ku genes disrupts the subnuclear organization of telomeres. *Curr. Biol.* 8:653–656. doi:10.1016/S0960-9822(98)70252-0
- Lees-Miller, S.P., K. Sakaguchi, S.J. Ullrich, E. Appella, and C.W. Anderson. 1992. Human DNA-activated protein kinase phosphorylates serines 15 and 37 in the amino-terminal transactivation domain of human p53. *Mol. Cell Biol.* 12:5041–5049.
- Li, H., S.H. Li, H. Johnston, P.F. Shelbourne, and X.J. Li. 2000. Amino-terminal fragments of mutant huntingtin show selective accumulation in striatal neurons and synaptic toxicity. *Nat. Genet.* 25:385–389. doi:10.1038/78054
- Li, L., T.H. Murphy, M.R. Hayden, and L.A. Raymond. 2004. Enhanced striatal NR2B-containing N-methyl-D-aspartate receptor-mediated synaptic currents in a mouse model of Huntington disease. *J. Neurophysiol.* 92:2738–2746. doi:10.1152/jn.00308.2004
- Lieber, M.R., Y. Ma, U. Pannicke, and K. Schwarz. 2003. Mechanism and regulation of human non-homologous DNA end-joining. *Nat. Rev. Mol. Cell Biol.* 4:712–720. doi:10.1038/nrm1202
- Lim, J., T. Hao, C. Shaw, A.J. Patel, G. Szabó, J.F. Rual, C.J. Fisk, N. Li, A. Smolyar, D.E. Hill, et al. 2006. A protein-protein interaction network for human inherited ataxias and disorders of Purkinje cell degeneration. *Cell*. 125:801–814. doi:10.1016/j.cell.2006.03.032
- Lim, J., J. Crespo-Barreto, P. Jafar-Nejad, A.B. Bowman, R. Richman, D.E. Hill, H.T. Orr, and H.Y. Zoghbi. 2008. Opposing effects of polyglutamine expansion on native protein complexes contribute to SCA1. *Nature*. 452:713–718. doi:10.1038/nature06731
- Lin, M.T., and M.F. Beal. 2006. Mitochondrial dysfunction and oxidative stress in neurodegenerative diseases. *Nature*. 443:787–795. doi:10.1038/nature05292
- Lombard, D.B., K.F. Chua, R. Mostoslavsky, S. Franco, M. Gostissa, and F.W. Alt. 2005. DNA repair, genome stability, and aging. *Cell*. 120:497–512. doi:10.1016/j.cell.2005.01.028

- Lu, C., F. Zhu, Y.Y. Cho, F. Tang, T. Zykova, W.Y. Ma, A.M. Bode, and Z. Dong. 2006. Cell apoptosis: requirement of H2AX in DNA ladder formation, but not for the activation of caspase-3. *Mol. Cell.* 23:121–132. doi:10.1016/j.molcel.2006.05.023
- Mangiarini, L., K. Sathasivam, M. Seller, B. Cozens, A. Harper, C. Hetherington, M. Lawton, Y. Trotter, H. Leirach, S.W. Davies, and G.P. Bates. 1996. Exon 1 of the HD gene with an expanded CAG repeat is sufficient to cause a progressive neurological phenotype in transgenic mice. *Cell.* 87:493–506. doi:10.1016/S0092-8674(00)81369-0
- Martin, S.G., T. Laroche, N. Suka, M. Grunstein, and S.M. Gasser. 1999. Relocalization of telomeric Ku and SIR proteins in response to DNA strand breaks in yeast. *Cell.* 97:621–633. doi:10.1016/S0092-8674(00)80773-4
- Metzler, M., V. Legendre-Guillemain, L. Gan, V. Chopra, A. Kwok, P.S. McPherson, and M.R. Hayden. 2001. HIP1 functions in clathrin-mediated endocytosis through binding to clathrin and adaptor protein 2. *J. Biol. Chem.* 276:39271–39276. doi:10.1074/jbc.C100401200
- Murphy, K.P., R.J. Carter, L.A. Lione, L. Mangiarini, A. Mahal, G.P. Bates, S.B. Dunnett, and A.J. Morton. 2000. Abnormal synaptic plasticity and impaired spatial cognition in mice transgenic for exon 1 of the human Huntington's disease mutation. *J. Neurosci.* 20:5115–5123.
- Okazawa, H. 2003. Polyglutamine diseases: a transcription disorder? *Cell. Mol. Life Sci.* 60:1427–1439. doi:10.1007/s00018-003-3013-z
- Okazawa, H., T. Rich, A. Chang, X. Lin, M. Waragai, M. Kajikawa, Y. Enokido, A. Komuro, S. Kato, M. Shibata, et al. 2002. Interaction between mutant ataxin-1 and PQBP-1 affects transcription and cell death. *Neuron.* 34:701–713. doi:10.1016/S0896-6273(02)00697-9
- Olive, P.L., and J.P. Banáth. 2006. The comet assay: a method to measure DNA damage in individual cells. *Nat. Protoc.* 1:23–29. doi:10.1038/nprot.2006.5
- Orii, K.E., Y. Lee, N. Kondo, and P.J. McKinnon. 2006. Selective utilization of nonhomologous end-joining and homologous recombination DNA repair pathways during nervous system development. *Proc. Natl. Acad. Sci. USA.* 103:10017–10022. doi:10.1073/pnas.0602436103
- Oshima, J., C.E. Yu, C. Piussan, G. Klein, J. Jabkowski, S. Balci, T. Miki, J. Nakura, T. Ogihara, J. Ellis, et al. 1996. Homozygous and compound heterozygous mutations at the Werner syndrome locus. *Hum. Mol. Genet.* 5:1909–1913. doi:10.1093/hmg/5.12.1909
- Pandey, U.B., Z. Nie, Y. Batlevi, B.A. McCray, G.P. Ritson, N.B. Nedelsky, S.L. Schwartz, N.A. DiProspero, M.A. Knight, O. Schuldiner, et al. 2007. HDAC6 rescues neurodegeneration and provides an essential link between autophagy and the UPS. *Nature.* 447:859–863. doi:10.1038/nature05853
- Panov, A.V., C.A. Gutekunst, B.R. Leavitt, M.R. Hayden, J.R. Burke, W.J. Strittmatter, and J.T. Greenamyre. 2002. Early mitochondrial calcium defects in Huntington's disease are a direct effect of polyglutamines. *Nat. Neurosci.* 5:731–736.
- Qi, M.L., K. Tagawa, Y. Enokido, N. Yoshimura, Y. Wada, K. Watase, S. Ishiura, I. Kanazawa, J. Botas, M. Saitoe, et al. 2007. Proteome analysis of soluble nuclear proteins reveals that HMGB1/2 suppress genotoxic stress in polyglutamine diseases. *Nat. Cell Biol.* 9:402–414. doi:10.1038/ncb1553
- Ravikumar, B., C. Vacher, Z. Berger, J.E. Davies, S. Luo, L.G. Oroz, F. Scaravilli, D.F. Easton, R. Duden, C.J. O'Kane, and D.C. Rubinsztein. 2004. Inhibition of mTOR induces autophagy and reduces toxicity of polyglutamine expansions in fly and mouse models of Huntington disease. *Nat. Genet.* 36:585–595. doi:10.1038/ng1362
- Ribes-Zamora, A., I. Mihalek, O. Lichtarge, and A.A. Bertuch. 2007. Distinct faces of the Ku heterodimer mediate DNA repair and telomeric functions. *Nat. Struct. Mol. Biol.* 14:301–307. doi:10.1038/nsmb1214
- Riha, K., J.M. Watson, J. Parkey, and D.E. Shippen. 2002. Telomere length deregulation and enhanced sensitivity to genotoxic stress in *Arabidopsis* mutants deficient in Ku70. *EMBO J.* 21:2819–2826. doi:10.1093/emboj/21.11.2819
- Ross, C.A., and L.M. Thompson. 2006. Transcription meets metabolism in neurodegeneration. *Nat. Med.* 12:1239–1241. doi:10.1038/nm1106-1239
- Roze, E., S. Betuing, C. Deyts, E. Marcon, K. Brami-Cherrier, C. Pagès, S. Humbert, K. Mérianne, and J. Caboche. 2008. Mitogen- and stress-activated protein kinase-1 deficiency is involved in expanded-huntingtin-induced transcriptional dysregulation and striatal death. *FASEB J.* 22:1083–1093. doi:10.1096/fj.07-9814
- Ruan, Q., M. Lesort, M.E. MacDonald, and G.V. Johnson. 2004. Striatal cells from mutant huntingtin knock-in mice are selectively vulnerable to mitochondrial complex II inhibitor-induced cell death through a non-apoptotic pathway. *Hum. Mol. Genet.* 13:669–681. doi:10.1093/hmg/ddh082
- Sancar, A., L.A. Lindsey-Boltz, K. Unsal-Kaçmaz, and S. Linn. 2004. Molecular mechanisms of mammalian DNA repair and the DNA damage checkpoints. *Annu. Rev. Biochem.* 73:39–85. doi:10.1146/annurev.biochem.73.011303.073723
- Saudou, F., S. Finkbeiner, D. Devys, and M.E. Greenberg. 1998. Huntingtin acts in the nucleus to induce apoptosis but death does not correlate with the formation of intranuclear inclusions. *Cell.* 95:55–66. doi:10.1016/S0092-8674(00)81782-1
- Sawa, A., A.A. Khan, L.D. Hester, and S.H. Snyder. 1997. Glyceraldehyde-3-phosphate dehydrogenase: nuclear translocation participates in neuronal and nonneuronal cell death. *Proc. Natl. Acad. Sci. USA.* 94:11669–11674. doi:10.1073/pnas.94.21.11669
- Sawada, H., H. Ishiguro, K. Nishii, K. Yamada, K. Tsuchida, H. Takahashi, J. Goto, I. Kanazawa, and T. Nagatsu. 2007. Characterization of neuron-specific huntingtin aggregates in human huntingtin knock-in mice. *Neurosci. Res.* 57:559–573. doi:10.1016/j.neures.2007.01.002
- Scherzinger, E., R. Lurz, M. Turmaine, L. Mangiarini, B. Hollenbach, R. Hasenbank, G.P. Bates, S.W. Davies, H. Lehrach, and E.E. Wanker. 1997. Huntingtin-encoded polyglutamine expansions form amyloid-like protein aggregates in vitro and in vivo. *Cell.* 90:549–558. doi:10.1016/S0092-8674(00)80514-0
- Schultz, L.B., N.H. Chehab, A. Malikzay, and T.D. Halazonetis. 2000. p53 binding protein 1 (53BP1) is an early participant in the cellular response to DNA double-strand breaks. *J. Cell Biol.* 151:1381–1390. doi:10.1083/jcb.151.7.1381
- Shibata, H., D.P. Huynh, and S.M. Pulst. 2000. A novel protein with RNA-binding motifs interacts with ataxin-2. *Hum. Mol. Genet.* 9:1303–1313. doi:10.1093/hmg/9.9.1303
- Siino, J.S., I.B. Nazarov, M.P. Svetlova, L.V. Solovjeva, R.H. Adamson, I.A. Zalenskaya, P.M. Yau, E.M. Bradbury, and N.V. Tomilin. 2002. Photobleaching of GFP-labeled H2AX in chromatin: H2AX has low diffusional mobility in the nucleus. *Biochem. Biophys. Res. Commun.* 297:1318–1323. doi:10.1016/S0006-291X(02)02383-5
- Singaraja, R.R., S. Hadano, M. Metzler, S. Givan, C.L. Wellington, S. Warby, A. Yanai, C.A. Gutekunst, B.R. Leavitt, H. Yi, et al. 2002. HIP14, a novel ankyrin domain-containing protein, links huntingtin to intracellular trafficking and endocytosis. *Hum. Mol. Genet.* 11:2815–2828. doi:10.1093/hmg/11.23.2815
- Sittler, A., R. Lurz, G. Lueder, J. Priller, H. Lehrach, M.K. Hayer-Hartl, F.U. Hartl, and E.E. Wanker. 2001. Geldanamycin activates a heat shock response and inhibits huntingtin aggregation in a cell culture model of Huntington's disease. *Hum. Mol. Genet.* 10:1307–1315. doi:10.1093/hmg/10.12.1307
- Soong, B.W., and H.L. Paulson. 2007. Spinocerebellar ataxias: an update. *Curr. Opin. Neurol.* 20:438–446. doi:10.1097/WCO.0b013e3281fbd3dd
- Sordet, O., C.E. Redon, J. Guirouilh-Barbat, S. Smith, S. Solier, C. Douarre, C. Conti, A.J. Nakamura, B.B. Das, E. Nicolas, et al. 2009. Ataxia telangiectasia mutated activation by transcription- and topoisomerase I-induced DNA double-strand breaks. *EMBO Rep.* 10:887–893. doi:10.1038/embor.2009.97
- St-Pierre, J., S. Drori, M. Uldry, J.M. Silvaggi, J. Rhee, S. Jäger, C. Handschin, K. Zheng, J. Lin, W. Yang, et al. 2006. Suppression of reactive oxygen species and neurodegeneration by the PGC-1 transcriptional coactivators. *Cell.* 127:397–408. doi:10.1016/j.cell.2006.09.024
- Steffan, J.S., A. Kazantsev, O. Spasic-Boskovic, M. Greenwald, Y.Z. Zhu, H. Gohler, E.E. Wanker, G.P. Bates, D.E. Housman, and L.M. Thompson. 2000. The Huntington's disease protein interacts with p53 and CREB-binding protein and represses transcription. *Proc. Natl. Acad. Sci. USA.* 97:6763–6768. doi:10.1073/pnas.100110097
- Stiff, T., M. O'Driscoll, N. Rief, K. Iwabuchi, M. Löbrich, and P.A. Jeggo. 2004. ATM and DNA-PK function redundantly to phosphorylate H2AX after exposure to ionizing radiation. *Cancer Res.* 64:2390–2396. doi:10.1158/0008-5472.CAN-03-3207
- Sugars, K.L., and D.C. Rubinsztein. 2003. Transcriptional abnormalities in Huntington disease. *Trends Genet.* 19:233–238. doi:10.1016/S0168-9525(03)00074-X
- Suraweera, A., O.J. Becherel, P. Chen, N. Rundle, R. Woods, J. Nakamura, M. Gatei, C. Criscuolo, A. Filla, L. Chessa, et al. 2007. Senataxin, defective in ataxia oculomotor apraxia type 2, is involved in the defense against oxidative DNA damage. *J. Cell Biol.* 177:969–979. doi:10.1083/jcb.200701042
- Tagawa, K., M. Hoshino, T. Okuda, H. Ueda, H. Hayashi, S. Engemann, H. Okado, M. Ichikawa, E.E. Wanker, and H. Okazawa. 2004. Distinct aggregation and cell death patterns among different types of primary neurons induced by mutant huntingtin protein. *J. Neurochem.* 89:974–987. doi:10.1111/j.1471-4159.2004.02372.x
- Tagawa, K., S. Marubuchi, M.L. Qi, Y. Enokido, T. Tamura, R. Inagaki, M. Murata, I. Kanazawa, E.E. Wanker, and H. Okazawa. 2007. The induction levels of heat shock protein 70 differentiate the vulnerabilities to mutant huntingtin among neuronal subtypes. *J. Neurosci.* 27:868–880. doi:10.1523/JNEUROSCI.4522-06.2007
- Takashima, H., C.F. Boerkoel, J. John, G.M. Saifi, M.A. Salih, D. Armstrong, Y. Mao, F.A. Quijcho, B.B. Roa, M. Nakagawa, et al. 2002. Mutation of TDP1, encoding a topoisomerase I-dependent DNA damage repair enzyme, in spinocerebellar ataxia with axonal neuropathy. *Nat. Genet.* 32:267–272. doi:10.1038/ng987

- The Huntington's Disease Collaborative Research Group. 1993. A novel gene containing a trinucleotide repeat that is expanded and unstable on Huntington's disease chromosomes. *Cell*. 72:971–983. doi:10.1016/0092-8674(93)90585-E
- Thomas, J.O., and A.A. Travers. 2001. HMG1 and 2, and related 'architectural' DNA-binding proteins. *Trends Biochem. Sci.* 26:167–174. doi:10.1016/S0968-0004(01)01801-1
- Tibbetts, R.S., K.M. Brumbaugh, J.M. Williams, J.N. Sarkaria, W.A. Cliby, S.Y. Shieh, Y. Taya, C. Prives, and R.T. Abraham. 1999. A role for ATR in the DNA damage-induced phosphorylation of p53. *Genes Dev.* 13:152–157. doi:10.1101/gad.13.2.152
- Tomimatsu, N., C.G. Tahimic, A. Otsuki, S. Burma, A. Fukuhara, K. Sato, G. Shiota, M. Oshimura, D.J. Chen, and A. Kurimasa. 2007. Ku70/80 modulates ATM and ATR signaling pathways in response to DNA double strand breaks. *J. Biol. Chem.* 282:10138–10145. doi:10.1074/jbc.M611880200
- Travers, A.A. 2003. Priming the nucleosome: a role for HMGB proteins? *EMBO Rep.* 4:131–136. doi:10.1038/sj.embor.embor741
- Troelstra, C., A. van Gool, J. de Wit, W. Vermeulen, D. Bootsma, and J.H. Hoeijmakers. 1992. ERCC6, a member of a subfamily of putative helicases, is involved in Cockayne's syndrome and preferential repair of active genes. *Cell*. 71:939–953. doi:10.1016/0092-8674(92)90390-X
- Venkatraman, P., R. Wetzel, M. Tanaka, N. Nukina, and A.L. Goldberg. 2004. Eukaryotic proteasomes cannot digest polyglutamine sequences and release them during degradation of polyglutamine-containing proteins. *Mol. Cell*. 14:95–104. doi:10.1016/S1097-2765(04)00151-0
- Wang, J.C. 2002. Cellular roles of DNA topoisomerases: a molecular perspective. *Nat. Rev. Mol. Cell Biol.* 3:430–440. doi:10.1038/nrm831
- Waragai, M., E. Junn, M. Kajikawa, S. Takeuchi, I. Kanazawa, M. Shibata, M.M. Mouradian, and H. Okazawa. 2000. PQBP-1/Npw38, a nuclear protein binding to the polyglutamine tract, interacts with U5-15kD/dim1p via the carboxyl-terminal domain. *Biochem. Biophys. Res. Commun.* 273:592–595. doi:10.1006/bbrc.2000.2992
- Weydt, P., V.V. Pineda, A.E. Torrence, R.T. Libby, T.F. Satterfield, E.R. Lazarowski, M.L. Gilbert, G.J. Morton, T.K. Bammler, A.D. Strand, et al. 2006. Thermoregulatory and metabolic defects in Huntington's disease transgenic mice implicate PGC-1alpha in Huntington's disease neurodegeneration. *Cell Metab.* 4:349–362. doi:10.1016/j.cmet.2006.10.004
- Wytenbach, A., O. Sauvageot, J. Carmichael, C. Diaz-Latoud, A.P. Arrigo, and D.C. Rubinsztein. 2002. Heat shock protein 27 prevents cellular polyglutamine toxicity and suppresses the increase of reactive oxygen species caused by huntingtin. *Hum. Mol. Genet.* 11:1137–1151. doi:10.1093/hmg/11.9.1137
- Yu, C.E., J. Oshima, Y.H. Fu, E.M. Wijsman, F. Hisama, R. Alisch, S. Matthews, J. Nakura, T. Miki, S. Ouais, et al. 1996. Positional cloning of the Werner's syndrome gene. *Science*. 272:258–262. doi:10.1126/science.272.5259.258
- Zhang, P., C. Dilley, and M.P. Mattson. 2007. DNA damage responses in neural cells: Focus on the telomere. *Neuroscience*. 145:1439–1448. doi:10.1016/j.neuroscience.2006.11.052

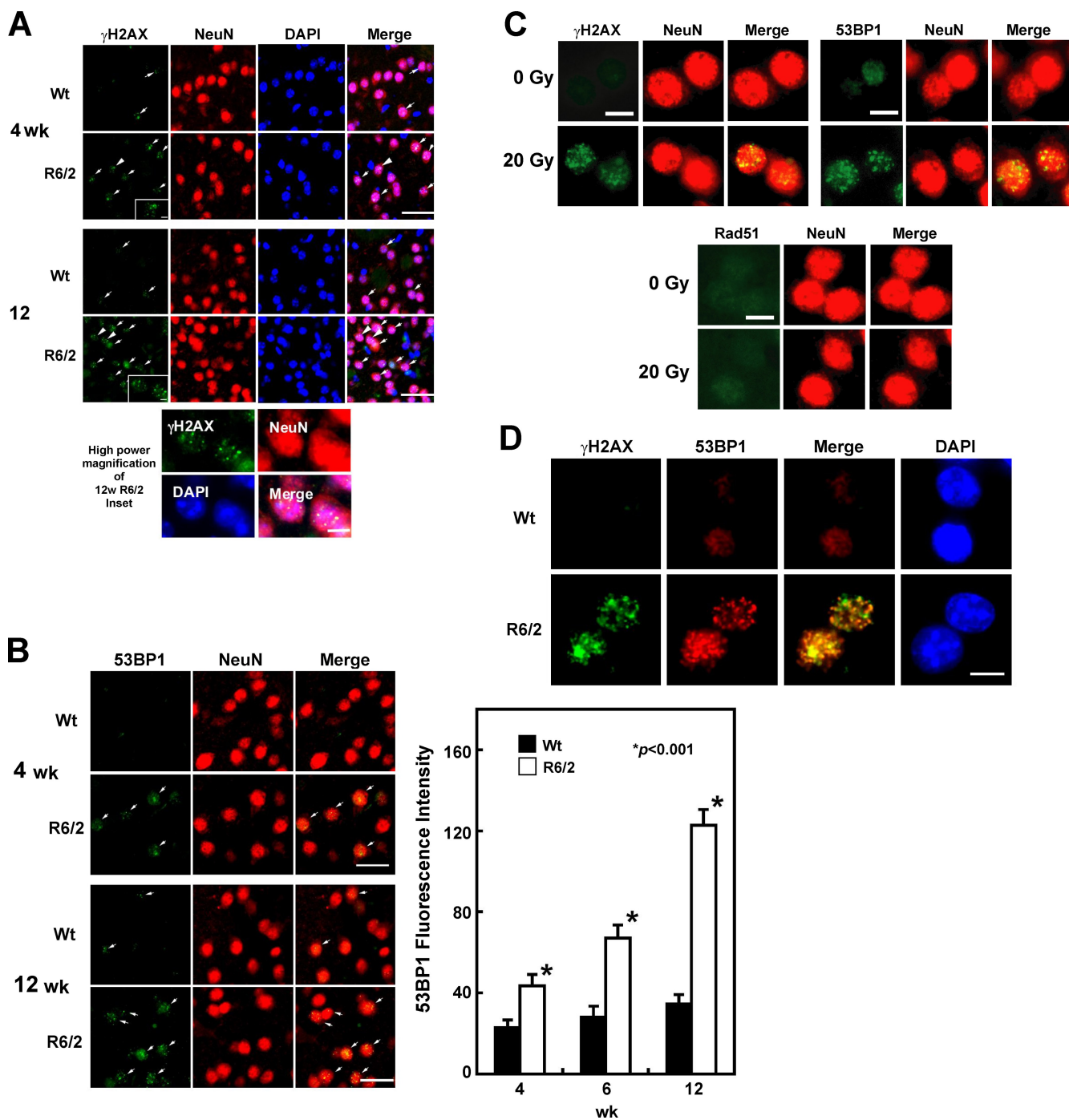
Enokido et al., <http://www.jcb.org/cgi/content/full/jcb.200905138/DC1>

Figure S1. **Activation of DSB marker proteins in striatal neurons in R6/2 mice.** (A) Triple staining with γ H2AX, NeuN, and DAPI shows foci formation of activated γ H2AX in the nuclei of striatal neurons of R6/2 mice. Arrows and arrowheads indicate striatal neurons showing γ H2AX activation. Insets and bottom panels show higher magnification views of stained neurons. Bars, 25 μ m. (B) Foci formation of 53BP1 in striatal neurons of R6/2 mice at 4, 6, and 12 wk of age. (right) Quantitative analysis ($n = 4$). *, $P < 0.01$ by Student's t test when compared with nontransgenic littermate (wild type [wt]). Bars, 25 μ m. (C) γ H2AX and 53BP1 immunostaining of striatal neurons of irradiated mouse brains. Bars, 25 μ m. (D) Costaining of γ H2AX and 53BP1 of striatal neurons in R6/2 mice. Foci of both molecules were merged. Bars, 10 μ m.

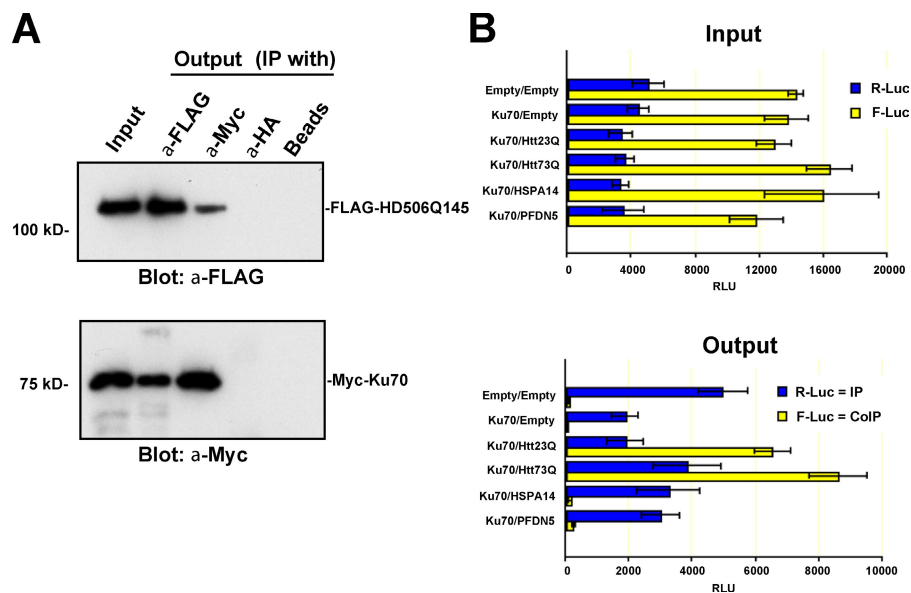


Figure S2. **Interaction between Ku70 and mutant Htt.** (A) IP assay showing the interaction between Ku70 and the full-length mutant Htt. Myc-Ku70 was coexpressed with Flag mutant full-length Htt (Flag-HD506Q145) in HEK293 cells and precipitated by anti-Flag, anti-Myc, or anti-HA (negative control) antibody. Nonspecific binding to beads is also shown as a negative control. (B) Binding assay with Renilla firefly luciferase activities shows the interaction between Htt and Ku70 in HEK293 cells. The interaction between Ku70 and Htt exon 1 fragment was tested using a LUMIER method. Protein A (PA)-Renilla luciferase-tagged (R-Luc) Ku70 and firefly luciferase (F-Luc)-tagged Htt fusion proteins were coexpressed in HEK293 cells, and cell extracts were assessed for the expression of the fusion proteins by measuring the R-Luc and F-Luc activity. (top) Renilla luciferase (R-Luc) and firefly luciferase (F-Luc) activities were used to quantify the expression of the fusion proteins in each coexpression. (bottom) Renilla luciferase activity was used to show the immunoprecipitation of PA-R-Luc fusion proteins. Firefly luciferase activity represented the binding (coprecipitation) of firefly fusion proteins with the R-Luc-fused Ku70. Mutant and wild-type Htt interact with Ku70 under overexpression of both proteins.

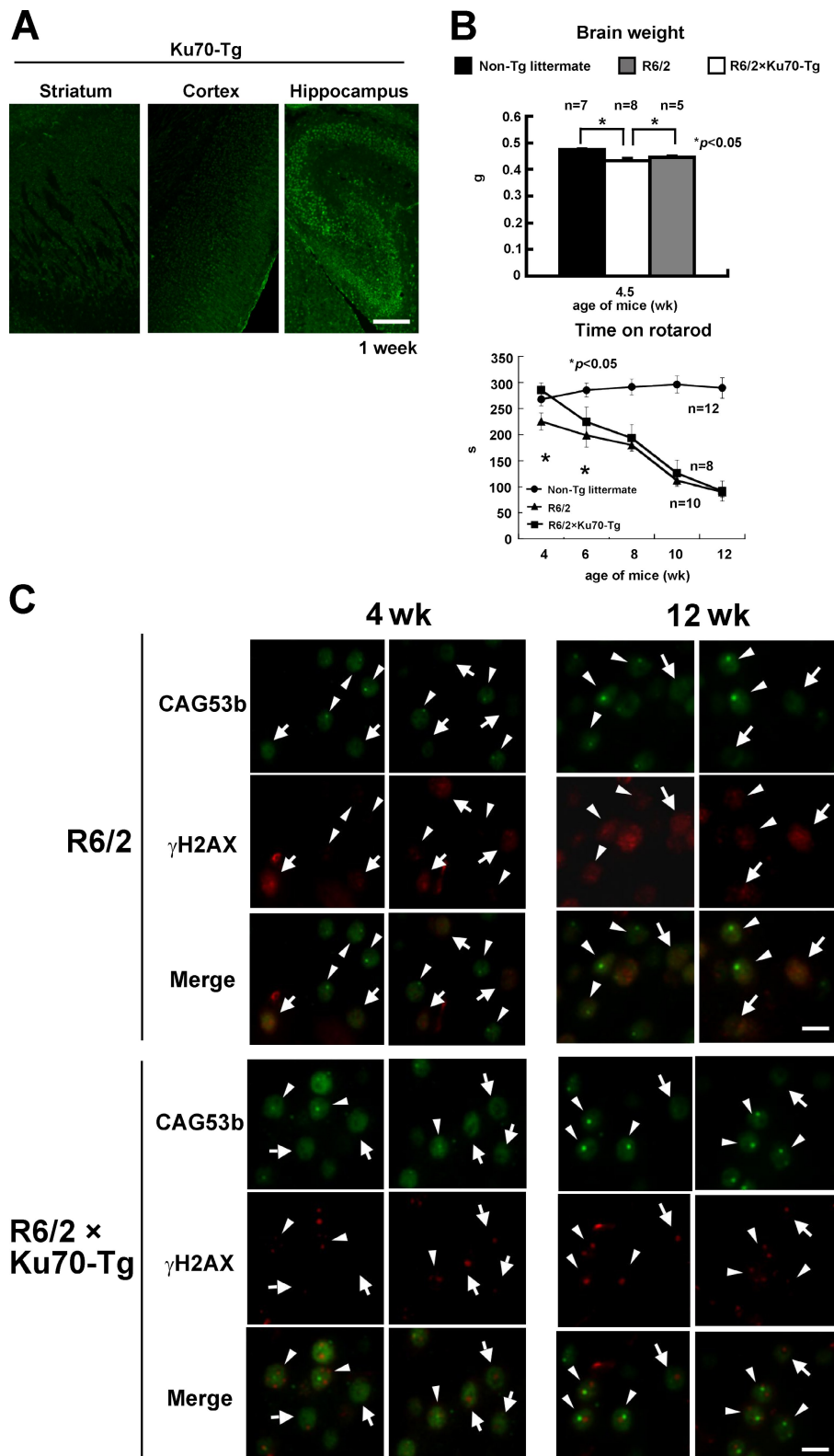


Figure S4. **Ku70 overexpression partially rescues mutant Htt toxicity in vivo.** (A) Immunohistochemistry with anti-Flag antibody confirmed expression of Ku70-Flag in the brain of Ku70 transgenic mice. The expression of Ku70-Flag protein was detected in cerebral cortex, striatum, and hippocampus of Ku70 transgenic mice by anti-Flag antibody. Bar, 50 μ m. (B) Effect of overexpression of Ku70 on brain weight and staying time on the rotarod. Both parameters showed mild improvement at 4.5 wk. (C) Higher magnification images of striatal neurons in mutant Htt transgenic (R6/2) and mutant Htt/Ku70 double-transgenic (R6/2 \times Ku70-Tg) mice are shown. Two representative images of striatal neurons costained with anti-Htt (CAG53b) and anti- γ H2AX antibodies from R6/2 and the double-transgenic mice at 4 and 12 wk. (left) In R6/2 mice at 4 wk, inclusion-positive neurons (arrowheads) show no signals of γ H2AX, whereas inclusion-negative neurons (arrows) show high shaggy signals. In striatal neurons of R6/2 \times Ku70 double-transgenic mice at 4 wk, the γ H2AX signals were localized to a few foci, and the background signals of γ H2AX in the nucleoplasm were very low in comparison with R6/2. In contrast to R6/2 mice, the γ H2AX staining pattern was not clearly different between inclusion-positive and -negative neurons. (right) In striatal neurons of R6/2 mice at 12 wk, γ H2AX signals were increased in comparison with R6/2 mice at 4 wk, in inclusion-positive neurons (arrowheads), and in inclusion-negative neurons (arrows). In double-transgenic mice at 12 wk, the γ H2AX signal of the nucleoplasm still remained at a low level, which is almost similar to the level of double-transgenic mice at 4 wk. Error bars indicate SEM. Bars, 10 μ m.

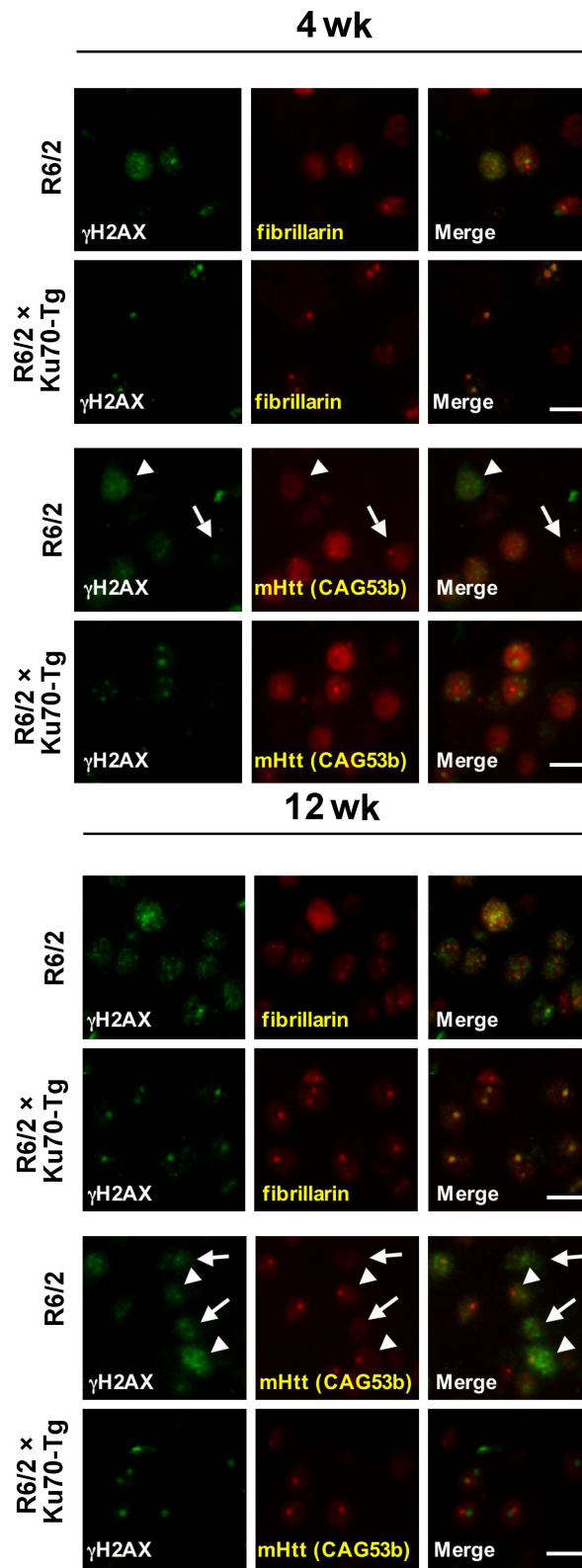


Figure S5. **Ku70 represses and relocates γ H2AX.** Costaining of striatal neurons of R6/2 and double-transgenic mice with anti- γ H2AX and antifibrillarin or anti-Htt (CAG53b) antibodies. The γ H2AX signals were localized to a few foci stained with a nucleolus marker, fibrillarin (top; 4 and 12 wk). The background signals of γ H2AX in the nucleoplasm were reduced in double-transgenic mice in comparison with R6/2 mice. (bottom) In R6/2 mice at 4 wk, inclusion-positive neurons (arrowheads) show lower signals of γ H2AX, whereas inclusion-negative neurons (arrows) show higher signals (4 wk). At 12 wk, the difference of γ H2AX between inclusion-positive and inclusion-negative neurons became unclear (12 wk). Bars, 15 μ m.

References

- Lescure, A., Y. Lutz, D. Eberhard, X. Jacq, A. Krol, I. Grummt, I. Davidson, P. Chambon, and L. Tora. 1994. The N-terminal domain of the human TATA-binding protein plays a role in transcription from TATA-containing RNA polymerase II and III promoters. *EMBO J.* 13:1166–1175.
- Scherzinger, E., R. Lurz, M. Turmaine, L. Mangiarini, B. Hollenbach, R. Hasenbank, G.P. Bates, S.W. Davies, H. Lehrach, and E.E. Wanker. 1997. Huntingtin-encoded polyglutamine expansions form amyloid-like protein aggregates in vitro and in vivo. *Cell.* 90:549–558. doi:10.1016/S0092-8674(00)80514-0